PLGA-BASED MOLECULAR CONTRAST AGENT FOR PPOCT AND VASCULAR-TARGETED MULTISTAGE DELIVERY SYSTEM

A Dissertation

by

JORGE ARTURO PALMA CHAVEZ

Submitted to the Office of Graduate and Professional Studies of
Texas A&M University
in partial fulfillment of the requirements for the degree of

DOCTOR OF PHILOSOPHY

Co-Chairs of Committee,	Javier A. Jo
	Phapanin P. Charoenphol
Committee Members,	Brian E. Applegate
	Kristen Maitland
	Akhilesh Gaharwar
Head of Department,	Mike McShane

May 2020

Major Subject: Biomedical Engineering

ABSTRACT

Atherosclerosis, a condition in which plaque accumulates on the inner wall of arteries, is often recognized as a precursor to cardiovascular diseases (CVDs), the most common causes of death in the US. Optical Coherence Tomography (OCT) is an optical diagnosis tool, which can be used to obtain high resolution morphological images of atherosclerotic plaque. However, atherosclerotic plaque vulnerability is often misclassified due to the signal similarities produced from different plaque components. An accurate plaque diagnosis is critical for the selection of treatments and procedures required to preserve the patients life. This thesis explores the fabrication and characterization of a vascular targeted MB-based contrast agent to enhance molecular imaging of Pump-Probe OCT (PPOCT).

Methylene blue (MB) was encapsulated into poly lactic-co-glycolic acid (PLGA) micro and nanoparticles by a single emulsion solvent evaporation method. The surface of particles was modified with ligands that can target molecular biomarkers involved in atherosclerotic plaque formation such as vascular cell adhesion molecules (VCAM-1) and apoptotic macrophages. Although nanoparticles have been extensively utilized as drug carriers due to their capabilities in intracellular localization, they exhibited poor margination in blood flow and consequently low concentrations at the vascular targets. Since microparticles (2-5 μm) have demonstrated significantly superior margination in human blood flows, a PLGA-based multistage delivery system (MDS) was developed to enable localization of nanoparticles to the vascular wall. This PLGA-based MDS consists of two stages: 1) a micron-sized outer shell and 2) encapsulated nanoparticles, aiming to achieve both effective margination and intracellular entry.

Overall, this study demonstrates the capabilities of MB particles as contrast agents for PPOCT and the potential of our Multi Stage Delivery System, as tools for atherosclerosis research and therapeutics.

DEDICATION

To my mother Silvia and my father Arturo whose unyielding love, sacrifice, support and encouragement enriched my soul and inspired me to pursue and complete this research.

ACKNOWLEDGMENTS

First, and most of all, I cannot express enough thanks to my advisors Dr. Phapanin Charoenphol and Dr. Javier Jo, for their assistance, guidance, encouragement and patience throughout the process of my PhD. I would like to thank my committee members, Dr. Brian Applegate, Dr. Kristen Maitland and Dr. Akhilesh Gaharwar, for their support, suggestions and encouragement along my studies.

I would also like to thank my colleagues Paritosh Pande, Shuna Cheng, Jose Rico Jimenez, Michael Serafino, Xi Chen, Yil-Hwan You, Elvis Duran, Ronald Juarez, Oscar Benavides, Priyanka Vasanthakumari, and Kevin Fuentes, for creating a welcoming environment, their mentorship in research and sharing their knowledge with me.

Thanks to my roommates Jose Rivera and Cesar Cobos, for their selfless friendship and great support.

Special thanks to my fiancée Valerie Briell, for her purest love and patience, for always cheer me up and stand by me through good and bad times.

Finally, I would like to thank God for blessing me with the most wonderful parents, Arturo Palma and Silvia Chavez, who raised me with tender love and exceptional values. You are always in my heart. To my sister Zulema Palma, for her love, patience, support and encouragement. I love you.

CONTRIBUTORS AND FUNDING SOURCES

Contributors

A dissertation committee consisting of Dr. Javier Jo (Chair), Dr. Brian Applegate, Dr. Kristen Maitland and Dr. Akhilesh Gaharwar of the Department of Biomedical Engineering and Dr. Phapanin Charoenphol (Co-Chair) of the Department of Mechanical Engineering.

The data analyzed in Chapter II and III was obtained in collaboration with Dr. Brian Applegates research group. The data studied in Chapter II, III and IV was obtained in collaboration with Dr. Phapanin Charoenphols research group.

Funding Sources

This graduate study was supported by the CONACyT fellowship, the American Hearth Association (AHA) (17SDG33660894), and the Cancer Prevention and Research Institute of Texas (CPRIT) (RP180588).

NOMENCLATURE

ACD	Acetate-Citrate-Dextrose
ADPA	Anthracene-9,10-Dipropionic Acid Disodium Salt
CCK-8	Colorimetric Cell Counting Kit-8
CNR	Contrast-to-Noise Ratio
CVD	Cardio Vascular Disease
DCM	Dichloromethane
DiO	3,3'-Dioctadecyloxacarbocyanine Perchlorate
DPBS	Dulbecco's Phosphate-Buffered Saline
EDAC	N-(3-Dimethylaminopropyl)-N-ethyl carbodiimide
ELISA	Enzyme-Linked Immunosorbent Assay
FDA	Food and Drug Administration
FFT	Fast Fourier Transform
FLIM	Fluorescence Lifetime Imaging
HUVEC	Human Umbilical Vein Endothelial Cells
IL-1	Interleukin 1 Beta
IVUS	Intravascular Ultrasound
LMB	Leucomethylene Blue
MB	Methylene Blue
MDS	Multistage Delivery System
MESF	Molecules of Equivalent Soluble Fluorochrome
NADH	Nicotinamide Adenine Dinucleotide
NTA	Nanoparticle Tracking Analysis

OCT	Optical Coherence Tomography
PEMA	Poly-Ethylene-Maleic Acid
PLGA	Poly-Lactic-co-Glycolic-Acid
PPFC	Parallel Plate Flow Chamber
PPOCT	Pump-Probe OCT
PVA	Poly-Vinyl Alcohol
RBC	Red Blood Cells
SD	Standard Deviation
SEM	Scanning Electron Microscopy
SLD	Super Luminescent Diode
SLeA	Sialyl Lewis A
VCAM-1	Vascular Cell Adhesion Molecule 1
WSR	Wall Shear Rate

TABLE OF CONTENTS

Page

ABSTRACT ii

DEDICATION iii

ACKNOWLEDGMENTS iv

CONTRIBUTORS AND FUNDING SOURCES v

NOMENCLATURE vi

TABLE OF CONTENTS viii

LIST OF FIGURES x

LIST OF TABLES xiii

1. INTRODUCTION 1

2. FABRICATION OF MB-BASED PPOCT CONTRAST AGENTS 3

2.1 Introduction 3
2.2 Materials and methods 5
2.2.1 Materials 5
2.2.2 Synthesis of methylene blue loaded PLGA particles (MB-PLGA) 5
2.2.3 Particle characterization 6
2.2.4 Methylene blue protection from enzymatic reduction 7
2.2.5 Singlet oxygen generation by encapsulated methylene blue 7
2.2.6 Characterization of MB particles as PPOCT contrast agents 8
2.3 Results 10
2.3.1 Synthesis and characterization of methylene blue loaded PLGA particles (MB-PLGA) 10
2.3.2 Effects of fabrication process parameters on particle morphology and methylene blue encapsulation efficiency 13
2.3.3 Methylene blue release profile from PLGA particles 15
2.3.4 PLGA particles form protective environment for MB from enzymatic reduction and prevent singlet oxygen release 16
2.3.5 In-vitro validation of MB-PLGA particles as PPOCT contrast agents 19
2.4 Discussion 21

3. FUNCTIONALIZATION OF MB-PLGA PARTICLES TO TARGET ATHEROSCLEROTIC PLAQUE BIOMARKERS 27

3.1 Introduction 27
3.2 Materials and Methods 28
3.2.1 Materials 28
3.2.2 Post Mortem Human Coronary Sections 28
3.2.3 Endothelium Permeability Test 29
3.2.4 Functionalization of PLGA Particles for Atherosclerotic Plaque Targeting 29
3.2.5 MB Microparticles Targeted to Ex-Vivo Human Artery Sections 31
3.3 Results 32
3.3.1 Endothelium Permeability Test 32
3.3.2 Conjugation of PLGA Particles to Vascular Endothelium Receptors 32
3.3.3 Ex-vivo Imaging of Atherosclerotic Human Arteries. 33
3.4 Discussion 34

4. MULTISTAGE DELIVERY SYSTEM 38

4.1 Introduction 38
4.2 Materials and Methods 40
4.2.1 Materials 40
4.2.2 Fabrication of Chitosan-Coated PLGA Nanospheres 40
4.2.3 Fabrication of PLGA-Based MDS 41
4.2.4 Isolation of RBCs, Cell-Free Plasma and Monocytes From Human Whole Blood 42
4.2.5 Culture of Human Umbilical Vein Endothelial Cells 43
4.2.6 MDS and Nanoparticle Cytotoxicity Study 43
4.2.7 Preparation of Ligand-Conjugated MDS and PLGA Nanoparticles 43
4.2.8 In-Vitro Flow Adhesion Experiment 44
4.3 Results 46
4.3.1 Chitosan-Coated PLGA Nanospheres 46
4.3.2 PLGA-Based Multistage Delivery Systems 47
4.3.3 In-Vitro Flow Adhesion Experiment 50
4.3.4 Discussion 51

5. CONCLUSIONS AND FUTURE WORK 57

5.1 Conclusions 57
5.2 Future Work 58

REFERENCES 59

LIST OF FIGURES

FIGURE Page

2.1 MB microparticles fabrication by an emulsification solvent evaporation method. 5

2.2 (A) Simplified energy level diagram of transient absorption. (B) PPOCT system schematic. 9

2.3 Schematic of the PPOCT image reconstruction algorithm. Interferograms are collected and processed via an inverse Fourier transform along wavenumber (k) to reconstruct OCT A-lines (z). M-scans are obtained by collecting A-lines from the same position in space at different time points ($S(z,t)$). A Fourier transform is applied to OCT M-scans along time (t) and the magnitude at the pump modulation frequency is extracted to form PPOCT B-scans ($S(z, f_{pump})$). 9

2.4 (A) Bright field microscopy image and (B) Scanning Electron microscopy (SEM) image of MB-PLGA microparticles (50:50 PLGA) with average diameter of 2.7 µm. (C) Scanning Electron microscopy (SEM) image and (D) NTA size distribution of MB nanoparticles (75:25 PLGA). 11

2.5 Absorption spectrum of methylene blue at different concentrations suspended in DI water. 12

2.6 Normalized absorption spectrum of MB solution, MB-PLGA microparticles (MB µp), and nanoparticles (MB np). 14

2.7 Effect of mechanical stir speed on MB-PLGA particle size. (A) Magnetic stirrer speed on 50:50 PLGA microparticles (3% surfactant, pH 8.4), (B) Sonicator tip resonance amplitude on 75:25 PLGA nanoparticles (3% surfactant, pH 8.4). Value = mean ± SD (n = 3). 15

2.8 Effect of continuous phase pH on MB encapsulation efficiency within PLGA microparticles and on particle size (50:50 PLGA, 3% surfactant). Value = mean ± SD (n = 3). 16

2.9 Methylene blue release from 50:50 PLGA microparticles and 50:50 and 75:25 PLGA nanoparticles in DPBS+ at pH 7.4, 37°C. Value = mean ± SD (n = 3). 17

2.10 Normalized MB fluorescence emission at 680 nm over time after addition of NADH enzyme to free MB, MB-PLGA microparticles and MB-PLGA nanoparticles in DI water. 18

2.11 Percentage of ADPA bleaching for free MB (no light) and irradiated free MB, MB-PLGA microparticles and MB-PLGA-nanoparticles with our pump 660 nm light source for 30 min. 20

2.12 PLGA microparticles loaded with different MB concentrations suspended in 200 µm capillary tubes. CNR scores for each MB microparticles batch. 21

2.13 PDMS microchannels of 500 µm diameter, were loaded with MB solution, MB microparticles and MB nanoparticles. Top row shows PPOCT B-Scan acquired with pump light source off. On the Bottom row, Pump was activated and MB molecules, either in solution or loaded inside of the polymeric spheres, were localized on the PPOCT B-Scan (blue). 22

3.1 Functionalization diagram of PLGA particle surface with biotinylated antibodies. ... 30

3.2 (A) Post-mortem human artery divided in 3 sections and treated with either MB solution (75 µg/mL), uncoated MB microparticles ($1x10^7$ p/mL) or a-VCAM1 functionalized MB-PLGA microparticles ($1x10^7$ p/mL) suspended in warm DPBS+. (B) 3D rendering of the custom-made flow chamber designed to hold human arterial sections and generate laminar flow over the artery lumen. 31

3.3 Confocal fluorescence microscope images of post-mortem human artery sections incubated with (A) DiO-PLGA microparticles, (B) DiD nanoparticles and (C) bright field overlaid. PPOCT images of an artery section (D) untreated, (E) MB microparticles and (F) MB nanoparticles. 33

3.4 Flow cytometry histogram of aVCAM-1 MB-PLGA microparticles labeled with a FITC-secondary antibody (blue) and uncoated MB-PLGA microparticles (gray). Fluorescence Intensity of an ELISA essay of functionalized micro and nanoparticles. 34

3.5 PPOCT (blue) overlaid on top of OCT (gray) images of ex vivo human coronary artery sections incubated with MB solution (top), uncoated MB microparticles (middle), or aVCAM-1 coated MB microparticles (bottom). 35

3.6 3D rendering of a PPOCT volume acquired by imaging a post-mortem human artery section treated with aVCAM-1 functionalized microparticles. (A) 3D-OCT, (B) Top-view PPOCT, (C) Cross-section PPOCT. 36

4.1 Schematic of the MDS drug-delivery strategy as a vascular-targeted microcarrier for PLGA nanoparticles. 39

4.2 Synthesis of MDS by a double emulsification solvent evaporation method. 42

4.3 (A) Circular parallel plate flow chamber. (B) Experimental setup used to test particle binding under laminar flow conditions. 45

4.4 SEM images of PLGA nanoparticles loaded with payload surrogate (DiO fluorescent dye) with an average diameter of (A) 78 nm, (B) 125 nm, (C) 207 nm and (D) 313 nm. 47

4.5 (A) Chitosan coating effect on PLGA nanoparticle surface zeta potential. (B) Methylene blue release profile of uncoated- and chitosan-coated nanoparticles in a saline buffer at 37°C. 48

4.6 MDS loaded with DiO nanoparticles fabricated by a double emulsion solvent evaporation method. MDS synthesized using different second emulsion homogenization speeds: (A) 12,500 rpm, (B) 8,500 rpm and (C) 6,500 rpm. The difference of shear stress applied during second emulsion resulted on drastic differences on MDS final diameter. MDS shown on (D) were prepared using same parameters than (C) except by a much higher shear stress applied during the first emulsification resulting in a honeycomb structure. 49

4.7 Fluorescent microscope images of MDS loaded with (A) 125 nm, (B) 206 nm and (C) 313 nm- DiO loaded nanoparticles. SEM cross-section images of MDS loaded with (D) 125 nm and (E) 313 nm DiO-loaded nanoparticles..... 53

4.8 MDS release profile in DPBS+ and Human Plasma at 37°C..... 54

4.9 Human monocytes cytotoxicity studies. Black bars represent human monocyte cell viability treated with media (control). Value = mean $\pm$ SD (n = 3). 54

4.10 HUVECs viability treated with control (media) and MDS at different concentrations. Value = mean $\pm$ SD (n = 3)..... 55

4.11 (A) Flow cytometry histogram of SLeA functionalized MDS labeled with a PE-secondary antibody (blue) and uncoated MDS (gray). (B) Fluorescence intensity from an ELISA essay of functionalized MDS and PLGA nanoparticles. 55

4.12 (A) Adhesion of sLeA or avidin-coated MDS to IL-1β-activated HUVECs monolayer under laminar flow in a parallel plate flow chamber and in the presence or absence of red blood cells (40% RBCs) (WSR = 100 s^{-1}). (B) Binding of MDS or PLGA nanoparticles, suspended in reconstituted blood (40% RBC), from flow to an activated HUVECs monolayer. Value = mean $\pm$ SD (n = 3). 56

LIST OF TABLES

TABLE Page

2.1 Fabrication parameters optimized to form MB loaded PLGA particles of the intended average diameters. 6

4.1 Average size of PLGA nanoparticles carrying methylene blue (MB) or DiO payloads. 46

4.2 Fabricated MDS carrying chitosan coated PLGA nanoparticles. 50

1. INTRODUCTION

This work was intended to provide a targeted molecular contrast agent as a tool to assist in the structural and molecular characterization of pathological tissues through Pump-Probe Optical Coherence Tomography (PPOCT) imaging. These polymeric platforms could facilitate the diagnosis of complex health conditions through optical imaging, and monitoring the transport and delivery of contrast agents and therapeutics to targeted locations. This dissertation consists of five chapters describing the development of targeted contrast agents for Pump-Probe OCT (PPOCT) and a Multistage Delivery System (MDS) microcarrier designed to enhance the delivery of nanoparticles into the vascular endothelium.

The first chapter briefly presents an introduction, the general scope of the experimental work and describes the organization of the dissertation.

The second chapter describes a fabrication method developed to prepare Poly-Lactic-co-Glycolic-Acid (PLGA) particles loaded with MB, and the methodology used to characterize their physical and chemical properties. The role of different fabrication parameters was explored in order to enhance the particle capabilities as PPOCT contrast agent. Phantoms were prepared and imaged to validate the PPOCT signal generated from encapsulated MB molecules.

The third chapter demonstrates the conjugation of PLGA particles to biotinylated antibodies, and introduces in-vitro and ex-vivo experiments to test the target specificity. Micro and nanoparticles were functionalized via carbodiimide chemistry with aVCAM-1 ligands and tested by flow-cytometry and ELISA essays. A custom-made flow chamber was designed to test the targeting of aVCAM-1 coated micro and nanoparticles to post-mortem human artery sections. Cross-sections and 3D images were reconstructed from the PPOCT B-scans acquired from tissues treated with aVCAM-1 targeted particles.

The fourth chapter investigates the development of MDS for the enhanced delivery of nanoparticles to the vascular endothelium. A new fabrication method was designed to load PLGA nanoparticles into PLGA microcapsules. MDS were functionalized with SLeA ligands, tested by flow-

cytometry, and validated by specific binding to IL1-β-activated HUVECs monolayer under an in-vitro flow experiment. Functionalized PLGA nanoparticles and MDS were targeted to an activated HUVECs monolayer to monitor and compare their vascular localization and binding efficiency as drug delivery technologies.

The fifth chapter draws the conclusion and summarizes the significant findings from this dissertation to the field of study. Several ideas are also proposed for future work.

2. FABRICATION OF MB-BASED PPOCT CONTRAST AGENTS

2.1 Introduction

Optical Coherence Tomography (OCT) is an optical technique used in research and clinical applications to obtain high-resolution cross-sectional images of various biological samples [1, 2, 3, 4, 5, 6]. In OCT, the image contrast is derived from samples variations in refractive index which allows morphological characterization of tissues. Since such variations are typically minimal among different type of biomolecules, a standard OCT is commonly merged with other complementary imaging tools or used with contrast agents to provide molecular imaging along with the morphological structure. Pump-probe OCT (PPOCT) is an integration of OCT with pump-probe spectroscopy, which is a technique that measures the transient absorption of a probe light source that is induced by molecular excitation through a pump light source [7, 8, 9, 10, 11]. This extension allows PPOCT to register molecular information from either endogenous or exogenous molecules. While endogenous contrast agents such as hemoglobin have been shown to provide molecular details to PPOCT, its efficiency is primarily limited by lack of specificity and moderate resolution due to interference from other comparable endogenous molecules [9, 10]. In contrast, exogenous agents can offer superior morphological contrast and specific labeling of biomarkers of interest.

Methylene blue (MB) is a phenothiazine dye that has been clinically approved for methemoglobinemia and malarial treatment and has been commonly used as a photosensitizer in photodynamic therapy [12, 13, 14, 15]. MB has a strong near-infrared absorption spectrum with a peak at 660 nm. With a strong spin-orbit coupling, MB molecules in the single excited state can easily populate the triplet ground state, which has a transient absorption band centered at 830 nm [9, 11]. To date, MB has been used as near infrared (NIR) fluorescence contrast guidance in many surgical procedures [16, 17] and has gained interest as an optical contrast for photoacoustic imaging [18, 19] and PPOCT [9, 11]. Our group demonstrated that soluble MB nonspecifically

accumulated in filtration organs of a zebrafish, and for the first time, provided molecular contrast for PPOCT imaging in vivo [11].

In general, an ideal contrast agent should highlight the specific biomarker location and have sufficient circulation lifetime during the imaging process. However, MB is known to be rapidly reduced to colorless and non-active leucomethylene blue (LMB) by biological enzymes [20, 21, 22]. Microencapsulation is a commonly used technique to prevent enzymatic reduction and to enable targeting specificity [23]. While several types of inorganic and organic carriers have been explored in PDT applications [24, 25, 26, 27], to our knowledge, no encapsulated MB formulation has been investigated as an optical imaging contrast agent.

Poly-lactic-co-glycolic acid (PLGA) is an FDA-approved biodegradable and biocompatible copolymer, which has been broadly used as a carrier for various contrast agents and/or therapeutics in clinical practice [28]. Due to their simple synthesis technique and tunable properties, PLGA particles can be fabricated with tailored properties such as size, shape, controlled payload delivery, and can successfully encapsulate both hydrophobic and hydrophilic agents [29, 30, 31]. Surface modification further allows controllability over particles interactions in biological environment. For instance, pegylation provides a steric hydrophilic layer on the particles, which avoids recognition from mononuclear phagocyte system and prolongs particle circulation lifetime. Modifying particle size and shape and labeling particle surface with targeting ligands allows particles to localize and accumulate in targeted tissues. Specifically, previous studies have demonstrated that sub-micron size (2-3 μm) exhibits optimal margination to the vascular wall in atherosclerotic flow environment, while nanoparticles (< 200 nm) are capable of penetrating into a permeable endothelial layer [32, 33, 34, 35].

The work presented here aims to develop MB-loaded PLGA microparticles (2-3 μm) and nanoparticles (100 nm) with controllable physical and optical properties. The capabilities of MB-PLGA particles as a PPOCT contrast agent were thoroughly evaluated in different conditions.

2.2 Materials and methods

2.2.1 Materials

Poly Lactic-co-Glycolic Acid (PLGA) (50:50 and 75:25) were acquired from Evonik Industries (Germany). Poly Ethylene-Maleic Acid (PEMA), Poly Vinyl Alcohol (PVA), Dulbeccos Phosphate Buffered Saline (DPBS), reduced dipotassium salt (NADH) and diaphorase from Clostridium Kluyveri (NADH dehydrogenase) were purchased from Sigma-Aldrich (US). Methylene Blue was obtained from Fisher Scientific (US). All reagent grade organic solvents were purchased from VWR (US).

2.2.2 Synthesis of methylene blue loaded PLGA particles (MB-PLGA)

MB-PLGA particles were fabricated by an oil-in-water (O/W) emulsion solvent evaporation method [36, 37, 38]. Briefly, an oil phase was prepared by dissolving methylene blue and PLGA polymer in dichloromethane (DCM). Then, the oil phase was injected dropwise into a continuous water phase containing poly-vinyl alcohol (PVA) and poly-ethylene-maleic Acid (PEMA) dissolved in DI water. PVA acts as a polymer stabilizer, which stabilizes the particles (droplets) and prevents aggregation. PEMA increases the number of carboxyl groups on the particle surface and thus, increasing available active sites for ligands functionalization [39]. During the emulsification process, the oil phase was broken into small droplets by shear stress produced either by a magnetic stir plate (Isotemp, Fisher Scientific) or a 20 kHz sonicator tip (Q125, QSonica), to form micro or nanoparticles respectively.

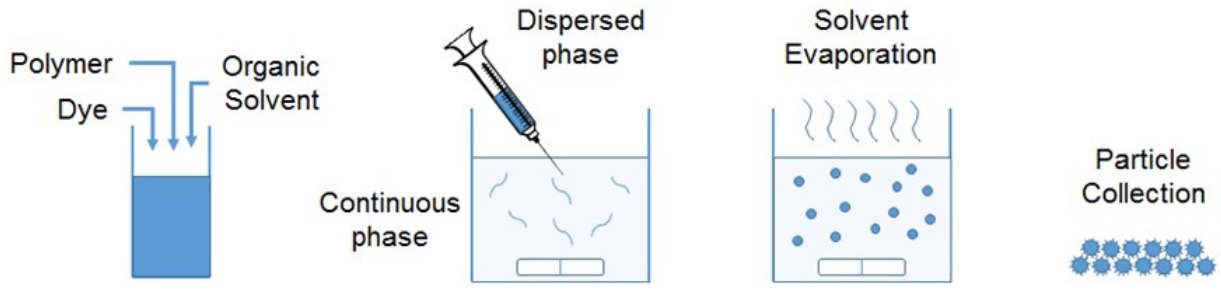

Figure 2.1: MB microparticles fabrication by an emulsification solvent evaporation method.

The emulsion mixture was stirred under a fume hood for 3 hours to ensure complete organic solvent evaporation and allow particles to solidify. The formed particles were washed, collected via centrifugation, and freeze-dried using a lyophilizer system (Freezone 2.5, LABCONCO). The dried MB-loaded particles were stored at -20°C in the dark until use. Relevant parameters used to prepare PLGA particles in this study are summarized in Table 1.

Parameter	Microparticles	Nanoparticles
Shear Stress	Stir Plate (1200 rpm)	1/8" Sonicator Tip (20 kHz - 25 W)
Polymer Concentration (Viscosity)	2 mg/mL	1 mg/mL
Emulsion Volume	90 mL	10 mL
Vol. of Reactor	200 mL	25 mL
Expected Avg. Diameter	**2-5 μm**	**80-100 nm**

Table 2.1: Fabrication parameters optimized to form MB loaded PLGA particles of the intended average diameters.

2.2.3 Particle characterization

Particles size and count were determined using a Nikon Eclipse 80i and a nanoparticle tracking analysis system (NanoSight LM10, Malvern Instruments). Particle surface charge was measured by zeta potential (Zetasizer Nanoseries, Malvern Instruments). Morphology of PLGA particles was verified by scanning electron microscopy (SEM Neoscope JCM-5000, Nikon). MB encapsulation of PLGA particles was determined via spectrometry by measuring particles light absorption at 665 nm and comparing against MB calibration solutions of known concentrations using a microplate reader (Synergy HTX, BioTek). MB encapsulation efficiency (EE_{MB}) was defined as the ratio of total MB obtained from dissolved particles divided by the initial amount of MB used during the particle fabrication process (2.1).

$$EE_{MB} = \frac{Mass\ loaded\ into\ particles}{Initial\ mass\ used\ during\ formulation} \times 100 \tag{2.1}$$

The release of MB from PLGA particles was monitored by incubating particles in phosphate buffered saline at 37°C, periodically collecting supernatant and resuspending particles in fresh buffer. The supernatants were analyzed via spectroscopy, to calculate the amount of MB released at each time point. Release rate of MB (RR_{MB}) was calculated as the cumulative mass of MB released over time divided by the total mass of MB loaded into the particles (2.2).

$$RR_{MB}(t) = \frac{Mass\ in\ supernatant\ (t)}{Total\ mass\ loaded\ into\ particles} \times 100 \tag{2.2}$$

2.2.4 Methylene blue protection from enzymatic reduction

Protection of methylene blue from enzymatic reduction was tested by a method previously reported [25, 26, 40]. Briefly, MB loaded PLGA particles and free soluble MB were prepared in 3 mL of Dulbeccos phosphate buffered saline (DPBS) (pH 7.4). NADH and diaphorase (NADH dehydrogenase), an enzyme present in red blood cells capable of reducing MB in vivo [41, 42], were sequentially added into the samples. Fluorescence intensity of MB at 680 nm was monitored for 1 hour using a photon-counting spectrofluorimeter (PC1, ISS). The fluorescence intensity of these solutions without NADH and diaphorase was used as a control. The reduction of MB into Leuco-MB was calculated as the decrease of fluorescence intensity over time $I_{MB}(t)$ after adding NADH dehydrogenase into the MB suspensions (2.3).

$$Enzymatic\ Reduction\ (t) = \frac{I_{MB}(0) - I_{MB}(t)}{I_{MB}(0)} \times 100 \tag{2.3}$$

2.2.5 Singlet oxygen generation by encapsulated methylene blue

The generation of singlet oxygen by MB-PLGA spheres, was verified using the ADPA method previously described [26]. MB loaded PLGA particles and free soluble MB were prepared in 2 mL of DPBS (pH 7.4) and mixed with 100 μM of Anthracene-9, 10-dipropionic acid disodium salt (ADPA), a singlet oxygen quencher commonly used to detect free radicals in a solution. The MB solutions were illuminated with our pump light source at 660 nm (2.5 mW) and samples were

periodically collected for up to 30 minutes. The fluorescence emission spectra of ADPA under excitation at 378 nm, was measured using a photon-counting spectrofluorimeter (PC1, ISS). The percentage of ADPA quenched was used to compare the amount of singlet oxygen generated from wither MB molecules in solution or encapsulated into PLGA particles.

$$Singlet\ Oxygen\ (t) = \frac{I_{ADPA}(0) - I_{ADPA}(t)}{I_{ADPA}(0)} \times 100 \tag{2.4}$$

2.2.6 Characterization of MB particles as PPOCT contrast agents

PPOCT integrates pump-probe spectroscopy, a molecular-sensitive technique commonly used to characterize materials, with spectral domain OCT. Pump-probe spectroscopy measures the transient absorption of a probe light source induced by molecular excitation of a sample through a pump light source. Transmission of pump light modulation to the probe absorption is considered a pump-probe signal. The PPOCT system used in this work was previously described in [11]. Briefly, the pump light source, a sinusoidal modulated 663 nm diode laser, was directed into the sample arm via a dichroic mirror. A super luminescent diode (SLD) centered at 830 nm was used as both the probe and the OCT light source and launched to a 2x2 fused fiber coupler to form a Michelson interferometer. Pump and probe were focused to a spot diameter of 19 μm and the sample was laterally scanned by a pair of galvo mirrors. A custom spectrometer was used as detector. Axial resolution of the system was 6 μm. The average light power delivered at the sample was 3.5 mW. The PPOCT system used in this project is illustrated in Fig. 2.2.

The spectral interferograms were processed generating OCT B-scans. Then, Fourier analysis was applied to OCT-MScan acquired from the same spatial location at different time points to extract the PPOCT signal at modulation frequency (4 KHz). OCT images and Pump Probe signal were processed in MATLAB and reconstructed by following the method described in [11]. Briefly, the collected interferograms ($S(k,t)$) were processed via an inverse Fourier transform along wavenumber (k) to reconstruct OCT A-Lines ($S(z,t)$). Then a Fourier transform was applied to OCT M-Scans ($S(z,f)$) along time (t) and the magnitude at the pump modulation frequency

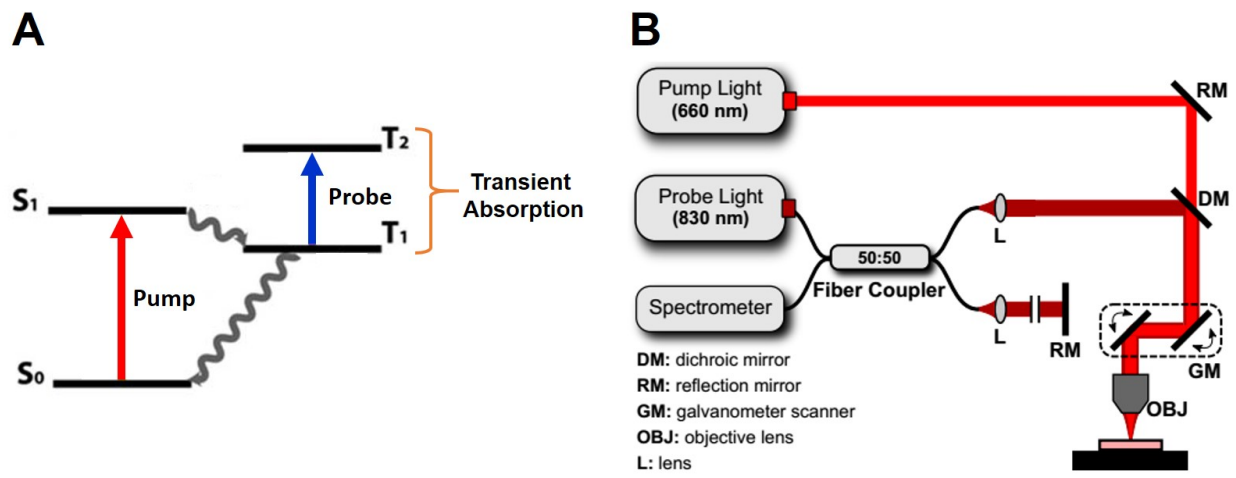

Figure 2.2: (A) Simplified energy level diagram of transient absorption. (B) PPOCT system schematic.

(f_{pump}) was extracted to reconstruct PPOCT B-Scans.

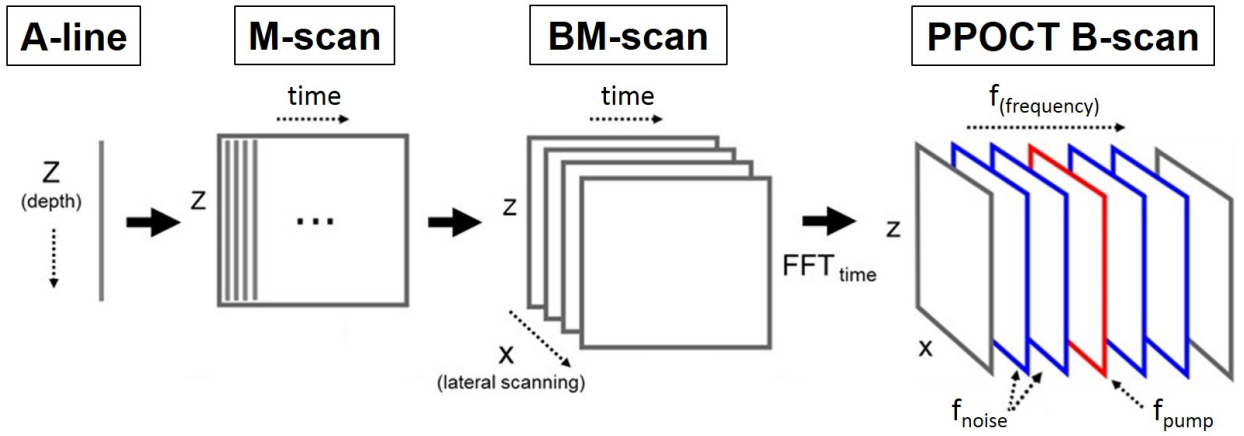

Figure 2.3: Schematic of the PPOCT image reconstruction algorithm. Interferograms are collected and processed via an inverse Fourier transform along wavenumber (k) to reconstruct OCT A-lines (z). M-scans are obtained by collecting A-lines from the same position in space at different time points ($S(z,t)$). A Fourier transform is applied to OCT M-scans along time (t) and the magnitude at the pump modulation frequency is extracted to form PPOCT B-scans ($S(z, f_{pump})$).

An in vitro setup was used to test and characterize the pump-probe signal generated from the

MB-based contrast agents. PLGA microparticles with inner MB concentrations of 8.9, 22.9 and 42.9 mM were suspended in DPBS and loaded into 200 μm inner diameter capillary tubes. Tubes were imaged using the PPOCT system with a pump power of 4.4 mW and probe power of 3.5 mW. PPOCT contrast-to-noise-ratio (CNR) was calculated as the ratio of the Pump-Probe signal amplitude at the modulation frequency ($A_{mod\ freq}$) divided by the mean of the Pump-Probe noise ($median\ A_{Noise}$) extracted from a band around the modulation frequency ($mod\ freq\ \pm 1\ KHz$).

$$Pump\ Probe\ CNR = \frac{A_{mod\ freq}}{median\ A_{Noise}} \tag{2.5}$$

Similarly, soluble MB, MB microparticles and MB nanoparticles were suspended in DPBS, and transferred into 500 μm diameter PDMS microchannels. The backscattering and pump-probe signals generated from the MB solutions and PLGA particles were evaluated by imaging with our PPOCT system.

2.3 Results

2.3.1 Synthesis and characterization of methylene blue loaded PLGA particles (MB-PLGA)

Methylene blue loaded PLGA particles were prepared by a modified single oil-in-water (O/W) emulsion solvent evaporation method. The base formulations consist of an oil phase containing 0.05-0.1 mg/mL of MB and 2.5-10 mg/mL of PLGA in dichloromethane, and a water phase containing 3 % of PVA-PEMA in DI water with a minimum pH of 4. By controlling a mechanical stir speed during the emulsification process, PLGA microparticles and nanoparticles were successfully synthesized with an average diameter of 2.7 μm (± 1 μm) and 84 nm (± 30 nm), respectively. These two particle sizes were chosen based on our previous studies and others, which demonstrates that 2-3 μm is an optimal particle size for targeting the vascular wall in atherosclerotic-flow condition, while nanoparticles sizes < 200 nm are suitable for penetrating into the arterial wall [32, 33, 34, 35]. The developed MB-PLGA micro- and nanoparticles are expected to optimally aid pump-probe optical coherence tomography (PPOCT) for molecular imaging on the vascular surface and within the atherosclerotic plaque.

Overall, MB-PLGA particles were produced at a rate of $1.44x10^{8}$ microparticles/hour and $4.22x10^{12}$ nanoparticles/hour using the modified O/W emulsion solvent evaporation method. Both microparticles and nanoparticles were spherical in shape with fairly smooth surfaces (Figure 2.4), and were fabricated with average MB encapsulation efficiencies of 82.6% and 48.4% for in microspheres and nanospheres, respectively.

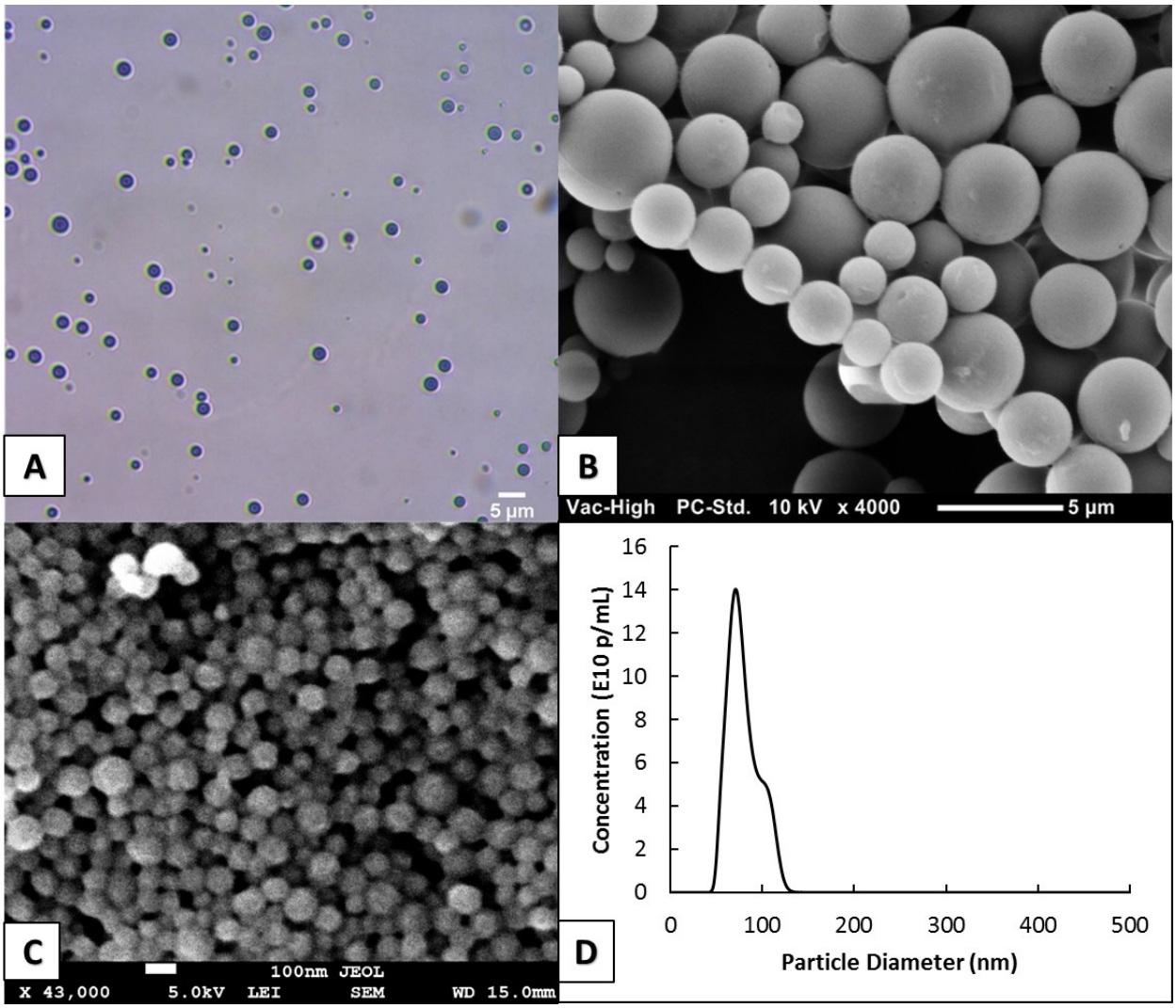

Figure 2.4: (A) Bright field microscopy image and (B) Scanning Electron microscopy (SEM) image of MB-PLGA microparticles (50:50 PLGA) with average diameter of 2.7 µm. (C) Scanning Electron microscopy (SEM) image and (D) NTA size distribution of MB nanoparticles (75:25 PLGA).

The physicochemical properties of MB-PLGA particles were determined by measuring their absorption spectra. MB is a cationic phenothiazine dye with an absorption peak at 664 nm in its monomeric form. At high concentration ($>$ 20 μM) or upon interaction with oppositely charged surface, MB tends to aggregate and form dimers, which exhibit a distinct absorption peak at 600 nm [43, 44]. The extent of MB dimerization can be evaluated by calculating the ratio of absorbance at 600 to 664 nm, namely a dimer to monomer ratio (D/M). Free MB (30 μM) had the D/M ratio of 0.61. As free MB concentration in solution increases from 20 μM to 200 μM, the D/M ratio increases from 0.59 to 1 (Fig. 2.5), as expected [45]. However, when free MB concentration is below 20 μM, increasing MB concentration does not affect the D/M ratio because dimers do not form at relative low MB concentration. Instead, higher MB concentration is favorable in this concentration range because it provides stronger absorbance intensity.

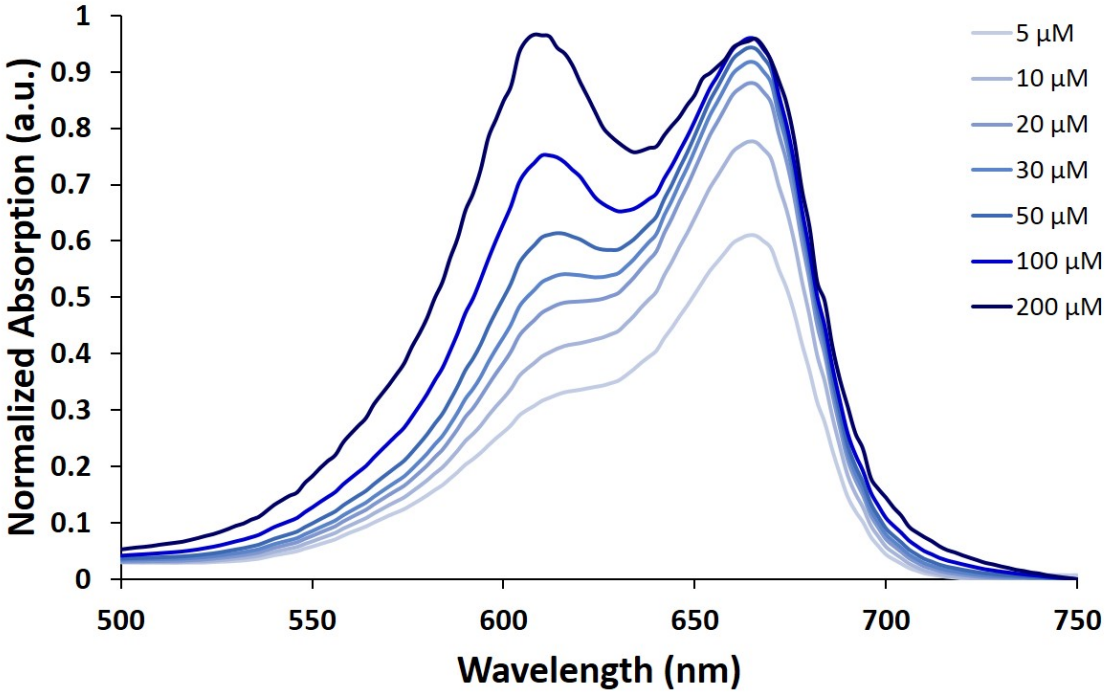

Figure 2.5: Absorption spectrum of methylene blue at different concentrations suspended in DI water.

Considering that each microparticle carries around 2.07x10^{-10} mg of MB and each nanosphere encapsulates 4.57x10^{-14} mg of MB, suspensions of 4.65x10^{7} microparticles and 2.1x10^{11} nanoparticles were prepared to match the total mass of MB dissolved in 1 mL of DI water at a concentration of 0.0096 mg/mL (30 μM). Figure 2.6 shows absorption spectra of free MB (30 μM or 0.0096 mg/mL), MB-PLGA microparticles (42.9 mM or 2.07x10^{-10} mg/particle) and MB-PLGA nanoparticles (40.6 mM or 4.57x10^{-14} mg/particle) in DI water. All MB formulations exhibit similar spectra, having a primary absorption peak at 664 nm and a secondary peak at 600 nm, which indicates the formation of both MB monomers and dimers in all cases. MB embedded in PLGA particles demonstrated higher D/M ratios relative to that of free MB, i.e. 0.87 in microparticles and 0.95 in nanoparticles compared to 0.61 in free MB (Fig. 2.6). This is likely because encapsulation decreases spatial distances among MB molecules and increases local MB concentration, which induces MB aggregation state within the particles. In addition, negatively charged COOH-PLGA polymer used in this study possibly further enhances MB aggregation as it can attract MB (positively charge in solution) binding to the surface [14, 38, 44]. Since the efficiency of PPOCT technique partially depends on the absorbance intensity of MB at the pump wavelength (660 nm), MB contrast agent formulation can be optimized by controlling the concentration of MB within the particles such that the monomeric form is maximal, and the dimeric form is minimal.

2.3.2 Effects of fabrication process parameters on particle morphology and methylene blue encapsulation efficiency

The emulsion solvent evaporation method has been widely used to fabricate various polymeric particles [36, 46]. Along with the mechanism of particle formation, several fabrication process parameters such as emulsification speed, surfactant concentration, polymer ratio, and viscosity and pH of the continuous phase, have been extensively investigated [29, 47, 48]. Similar to others, our study showed that the mechanical stir speed during the emulsification process dominantly control particle size. As the mechanical stir speed increases from 700 rpm to 1800 rpm, particle size decreases from 5.15 μm to 1.7 μm (Fig 2.7.A). The higher shear force generated by the increase in the stir speed causes the emulsified droplets to break up and yields smaller particles. Further

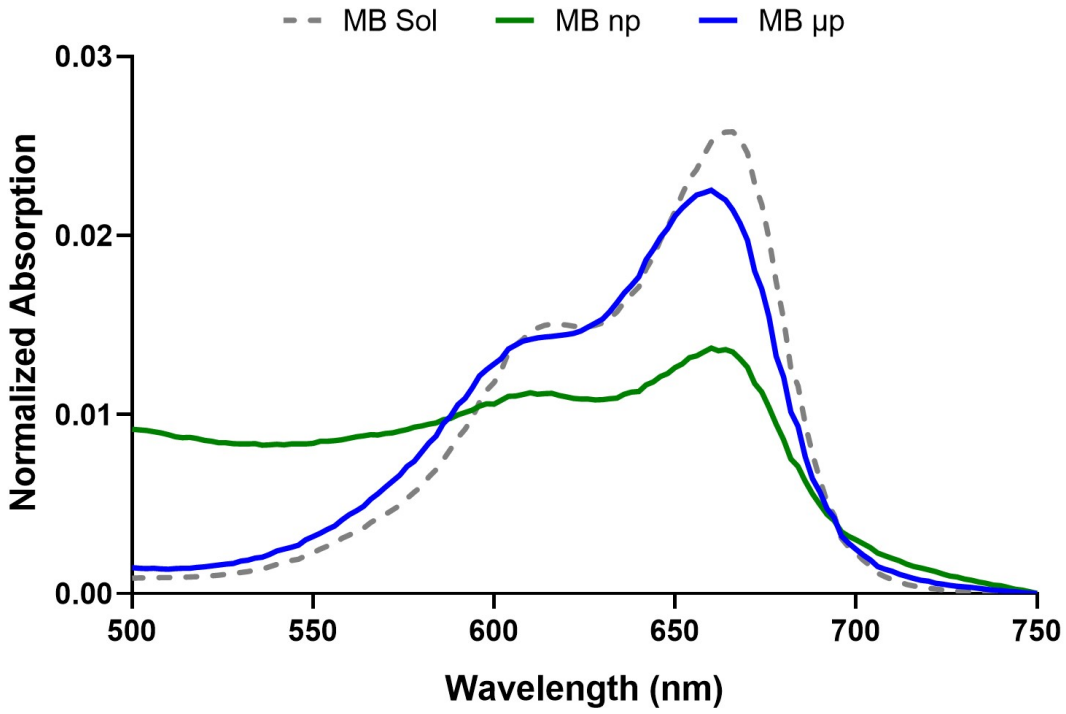

Figure 2.6: Normalized absorption spectrum of MB solution, MB-PLGA microparticles (MB µp), and nanoparticles (MB np).

increase in shear energy generated by a sonicator could reduce particle size down to 84 nm (Fig 2.7.B).

In addition to the stir speed, pH of the continuous aqueous phase significantly affect MB-PLGA particle formation and MB encapsulation efficiency. Since MB is a hydrophilic molecule, MB favorably partitioned out of the organic phase to the aqueous continuous phase during the emulsification and solvent evaporation process, resulting in relatively low MB encapsulation efficiency at neutral pH [49]. As pH increased from 6 to 8.4, encapsulation efficiency increased from 26% to 83% (Fig. 2.8). This is partially because the level of MB dimerization increases with the continuous phase pH [50]. The formation of MB dimers and MB aggregation in alkaline solution may delay and hinder MB molecules from leaking out of the polymer matrix during the fabrication process. Further increase to pH 10, however, resulted in decrease of encapsulation efficiency, while no significant difference in particle formation was observed between pH of 8.4 and 10. As also

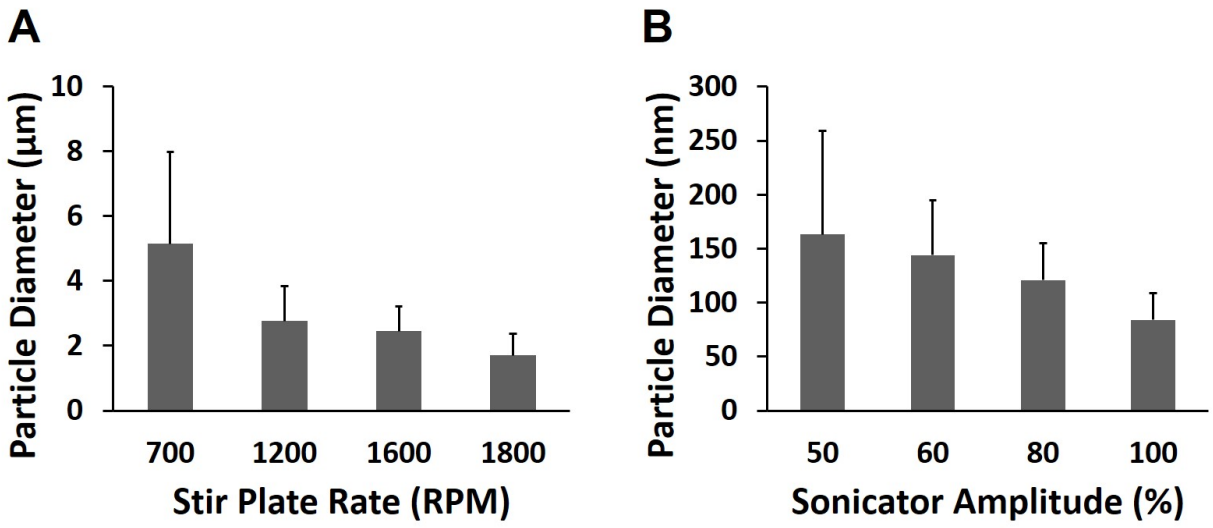

Figure 2.7: Effect of mechanical stir speed on MB-PLGA particle size. (A) Magnetic stirrer speed on 50:50 PLGA microparticles (3% surfactant, pH 8.4), (B) Sonicator tip resonance amplitude on 75:25 PLGA nanoparticles (3% surfactant, pH 8.4). Value = mean $\pm$ SD (n = 3).

shown in Fig. 2.8, the particle size was not affected by the change of the continuous phase pH. By using a water phase pH of 8.4, MB was encapsulated intro microparticles with an efficiency of 82.6%. Similarly, PLGA nanoparticles were fabricated using a water phase pH of 8.4 resulting in an encapsulation efficiency of 48.4%.

2.3.3 Methylene blue release profile from PLGA particles

Cumulative release of MB from PLGA micro and nanoparticles were studied in DPBS+ at pH 7.4 and 37°C for 24 hours. Considering the average procedural and imaging times of PPOCT are approximately two hours, MB release during this time window must be controlled to maintain sufficient MB signal throughout the process. As shown in Fig. 2.9, MB-PLGA (50:50) microparticles demonstrated a sustained release profile with 11% of total MB release in 2 hours. On the other hand, MB-PLGA (50:50) nanoparticles displayed a burst release profile with 81% of MB release in 2 hours (Fig. 2.9). The significant higher release rate from nanoparticles compared to microparticles is likely due to an increase in surface-to-volume ratio as particles become smaller. To reduce the amount of MB release, MB-PLGA nanoparticles were fabricated using 75:25 PLGA

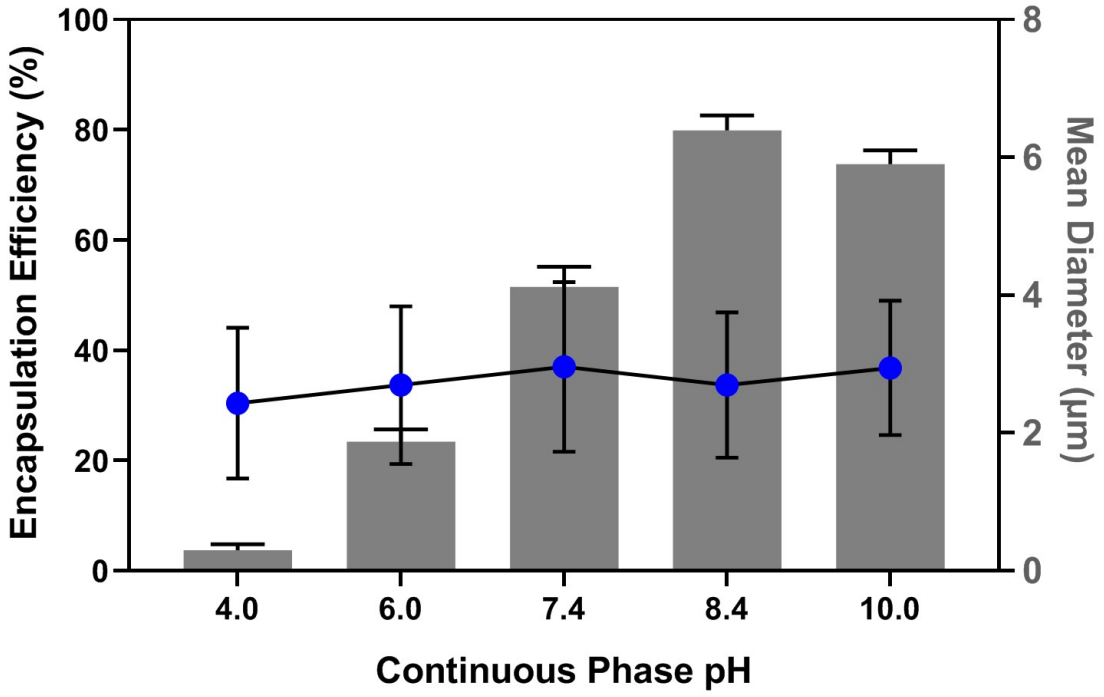

Figure 2.8: Effect of continuous phase pH on MB encapsulation efficiency within PLGA microparticles and on particle size (50:50 PLGA, 3% surfactant). Value = mean ± SD (n = 3).

polymer with the same base formulations. Fig. 2.9 shows that the MB release from 75:25 PLGA nanoparticles was significantly reduced particularly in the first few hours, i.e. 46% of total MB at 2 hours window. This result agrees with previous works reporting that a slower release profile associated with PLGA polymer with a higher lactic acid to glycolic acid ratio [47, 51].

2.3.4 PLGA particles form protective environment for MB from enzymatic reduction and prevent singlet oxygen release

The efficiency of MB as a contrast agent in biological environment is in part inhibited by its lack of target specificity and relatively short lifetime. In circulation, an average of 78% of MB is reduced by NADH/NADPH dehydrogenases and/or enzyme reductase in red blood cells and peripheral cells to colorless leukomethylene blue (LMB) [20, 21, 22]. LMB has negligible photodynamic activity and its spectral properties is invisible for our imaging system. Microencapsulation

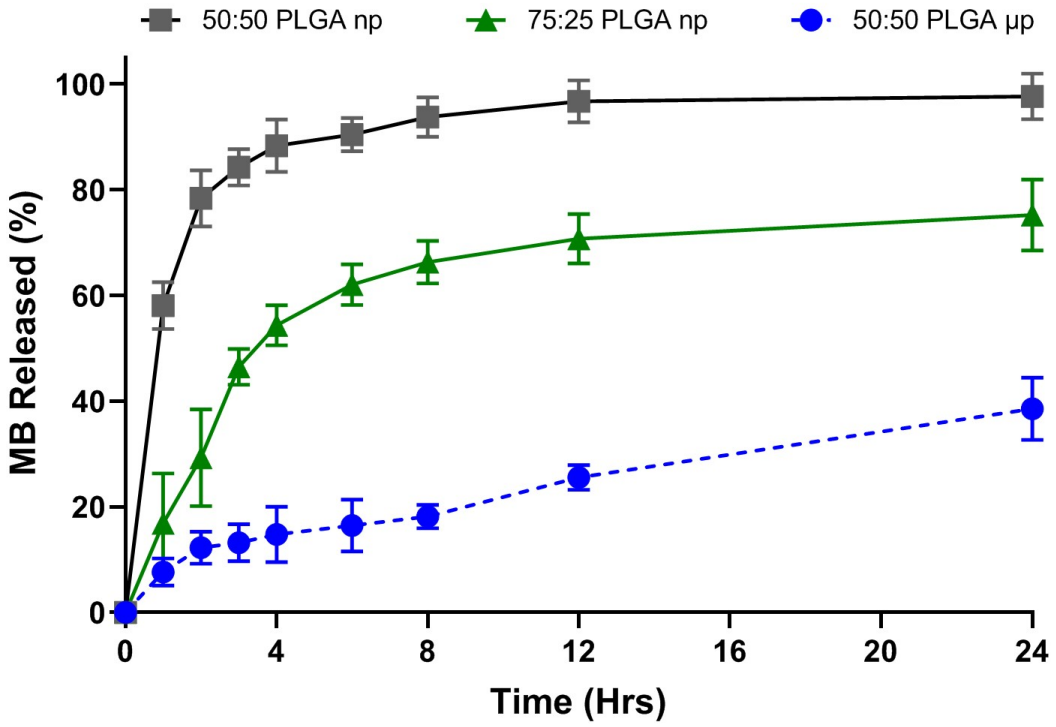

Figure 2.9: Methylene blue release from 50:50 PLGA microparticles and 50:50 and 75:25 PLGA nanoparticles in DPBS+ at pH 7.4, 37°C. Value = mean ± SD (n = 3).

technique has been used to increase MB target specificity and protect MB from the enzymatic reduction [26]. To the best of our knowledge, our MB-PLGA formulation as a PPOCT contrast agent is novel and needs to be assessed for the capacity to protect MB from the enzymatic reduction.

To mimic the enzyme activities in biological environment, free MB and MB-PLGA particles in DI water were sequentially incubated with NADH and diaphorase (NADH dehydrogenase) and the fluorescence intensity of MB at 680 nm was monitored for an hour. The decrease in fluorescence intensity indicates the reduction of MB into LMB, which does not exhibit emission at this wavelength. As shown in Fig. 2.10, approximately 96% of free MB was rapidly reduced within the first two minutes. In contrast, by encapsulating MB within PLGA particles, only 5% of MB in microparticles and 12% of MB in nanoparticles were reduced. These results indicate that a majority of MB remains immobilized within the PLGA matrix during the treatment and thus were provided a protective environment by the PLGA shell from the enzymatic reduction.

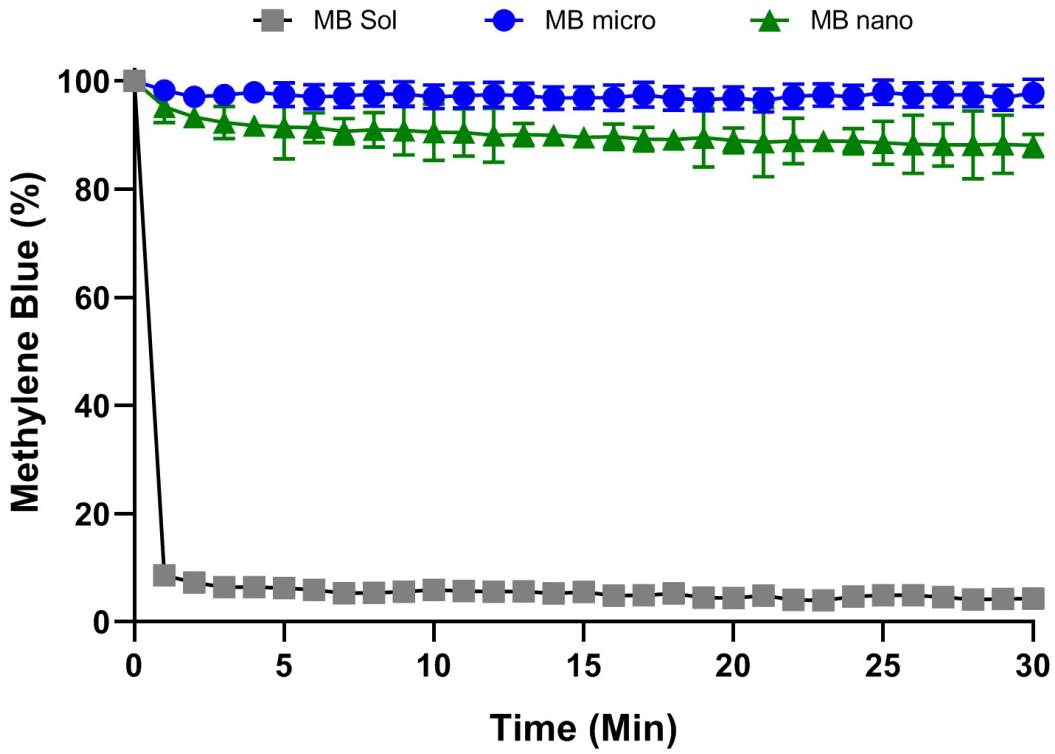

Figure 2.10: Normalized MB fluorescence emission at 680 nm over time after addition of NADH enzyme to free MB, MB-PLGA microparticles and MB-PLGA nanoparticles in DI water.

Primary properties of MB, which has captivated its utilization in therapeutic particularly in photodynamic therapy (PDT), include its FDA-approval, high quantum yield of singlet oxygen ($^1O_2$) generation in the therapeutic window (600-900 nm), and membrane permeability [52, 53]. In PDT, excited MB molecules in singlet and triplet stages generate reactive oxygen species (ROS), which irreversibly cause nearby cell damages. Although the $^1O_2$ generation is favorable in PDT for cancer treatment, it is an unfavorable product for PPOCT diagnosis and needs to be minimized. Similarly, microencapsulation is a potential approach to regulate $^1O_2$ local sequestration by controlling the polymeric network and the binding chemistry of MB within particles [24, 26, 54]. In this study, MB was entrapped within the PLGA polymeric matrix non-covalently. Our hypothesis was that MB-PLGA could potentially reduce, or at least delay, the local sequestration of $^1O_2$ to the surrounded environment. To test this hypothesis, free MB, MB-PLGA microparticles and

MB-PLGA nanoparticles were illuminated with the PPOCT pump light source at 660 nm for 30 min. The release of $^1O_2$ from irradiated MB to aqueous solution was monitored using a chemical probe, ADPA [24, 26]. Once ADPA reacts with $^1O_2$, it is irreversibly reduced into ADPA endoperoxide, which causes a decrease in the fluorescence emission of ADPA at 378 nm. The decrease in ADPA fluorescent intensity, reported as the percentage of ADPA bleaching in Fig. 2.11, indirectly estimates the efficiency of $^1O_2$ generation and release into surrounded environment. As previously shown in existing studies, free MB generates $^1O_2$ upon irradiation while exhibiting no cytotoxicity without illumination (i.e. low dark toxicity) [12, 25, 26]. In contrast, MB embedded within PLGA microparticles and nanoparticles favorably reduced the release of $^1O_2$ by 97% (34-fold) and 75% (4-fold) relative to that of free MB, respectively. This reduction is likely due to a quenching of the MB excited state and the formation of MB dimers within the polymer matrix, as shown in Fig. 2.6. MB dimers have a different absorption peak and thus do not produce $^1O_2$ upon 660 nm irradiation. This result shows that MB-PLGA particles can hinder the local sequestration of $^1O_2$, thus suppressing an adverse effect associated with MB utilization.

2.3.5 In-vitro validation of MB-PLGA particles as PPOCT contrast agents

MB microparticles loaded inside of 200 ţm inner diameter capillary tubes were imaged and their CNRs were estimated from the processed PPOCT B-Scans. PLGA microparticles loaded with 8.9, 22.9 and 42.9 mM MB, had CNRs of 4.43, 5.47 and 5.86, respectively (Fig. 2.12). Similar CNR trends were observed for nanoparticles. Based on CNR results, PLGA microspheres loaded with 42.9 mM MB and nanoparticles loaded with 40.6 mM MB are considered optimal formulations as PPOCT contrast agents.

In order to compare the PPOCT signal generated from MB solution, microparticles and nanoparticles, suspensions were prepared in DPBS and introduced into PDMS microchannels (500 µm diameter). The transient absorption of soluble or encapsulated methylene blue was recorded in a PPOCT B-Scan (Fig. 2.13). In the top row of Fig. 2.13, MB molecules were not localized since the pump light source was deactivated and transient absorption at the probe wavelength was not induced. On the other hand, in the bottom row of Fig. 2.13 encapsulated MB was illuminated by

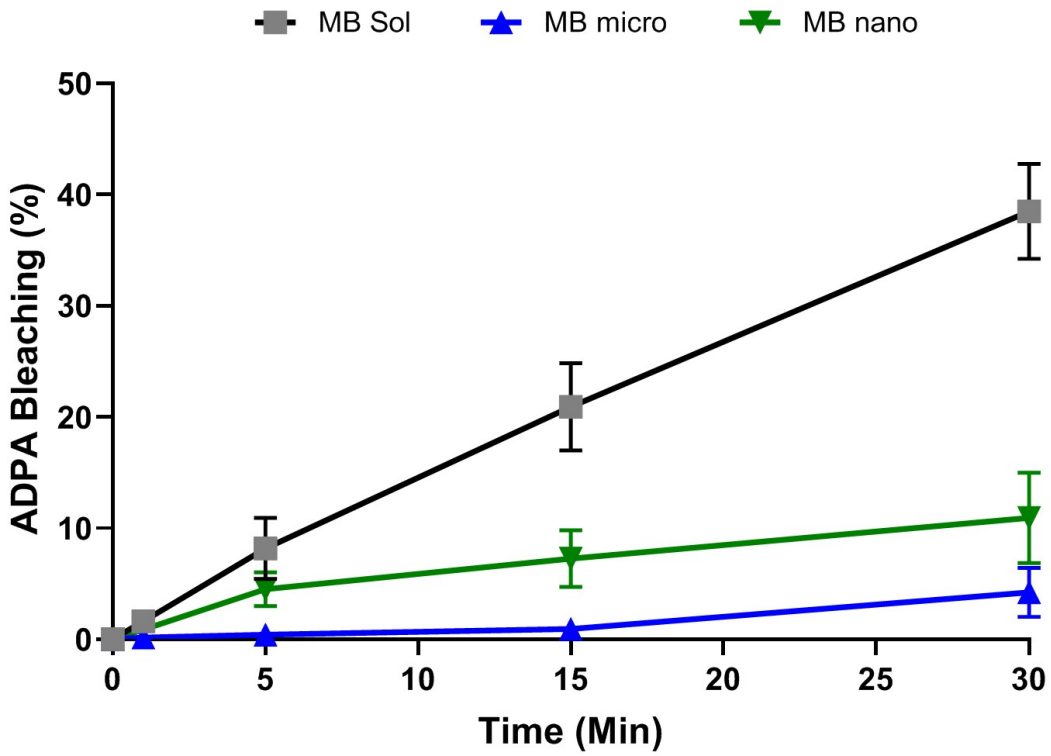

Figure 2.11: Percentage of ADPA bleaching for free MB (no light) and irradiated free MB, MB-PLGA microparticles and MB-PLGA-nanoparticles with our pump 660 nm light source for 30 min.

the modulated pump light source exciting MB molecules to a triplet state and enabling probe light absorption. Since pump-probe signal is encoded in the OCT interferogram, contrast is registered at the nearest backscattering material present in the sample. Due to this effect, signal produced from the MB solution was only visualized at the bottom surface of the microchannel. The lack of inherent scattering is one of the biggest drawbacks for chromophore solutions used as OCT contrast agents. In contrast, loading MB molecules inside of the particles polymeric shells provides extra backscattering and therefore an enhancement of the OCT signal. This allows to co-localize the OCT signal produced from the polymer shells with the Pump-Probe signal generated by the encapsulated MB molecules.

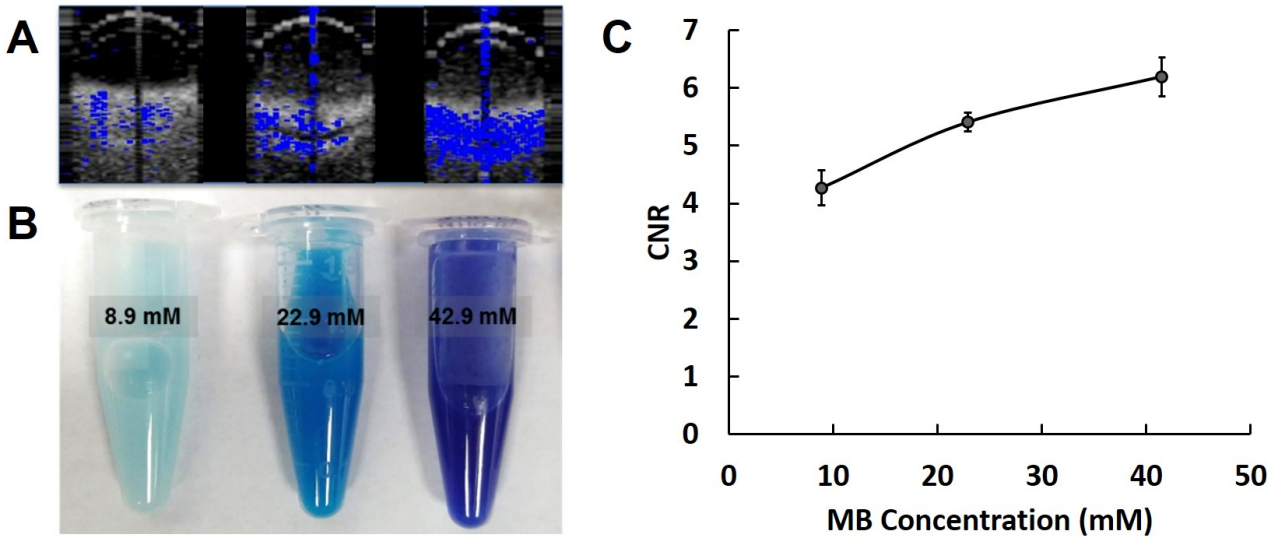

Figure 2.12: PLGA microparticles loaded with different MB concentrations suspended in 200 µm capillary tubes. CNR scores for each MB microparticles batch.

2.4 Discussion

Since the efficiency of particle localization on and within tissues has been shown to be size-dependent [32, 55], e.g. microparticles favor vascular surface targeting while nanoparticles favor intracellular penetration, the PLGA-based contrasts agents were fabricated into two size ranges (2.7 µm, 84 nm) to optimally target both locations (Fig. 2.4). Among the different fabrication parameters, the applied shear force during the emulsification process was demonstrated to primarily control the PLGA particle size in both micron and nanometer ranges. As the shear force increases, the external energy source provided to the organic phase to breakdown the emulsion droplet increases, thus decreasing the particle size. Other fabricating parameters such as oil phase viscosity, and oil phase/water phase volume ratios were also demonstrated to regulate particle size, particularly for smaller nanoparticles (< 100 nm). By increasing the oil phase viscosity and/or increasing the oil/water phase volume ratios, the viscous forces in the emulsified solution increases. Consequently, at a fixed external energy source, a net shear stress felt by the organic phase reduces, which results in an increase in the particle size.

In addition to the permeability of exogenous contrast agents through biological tissues, which

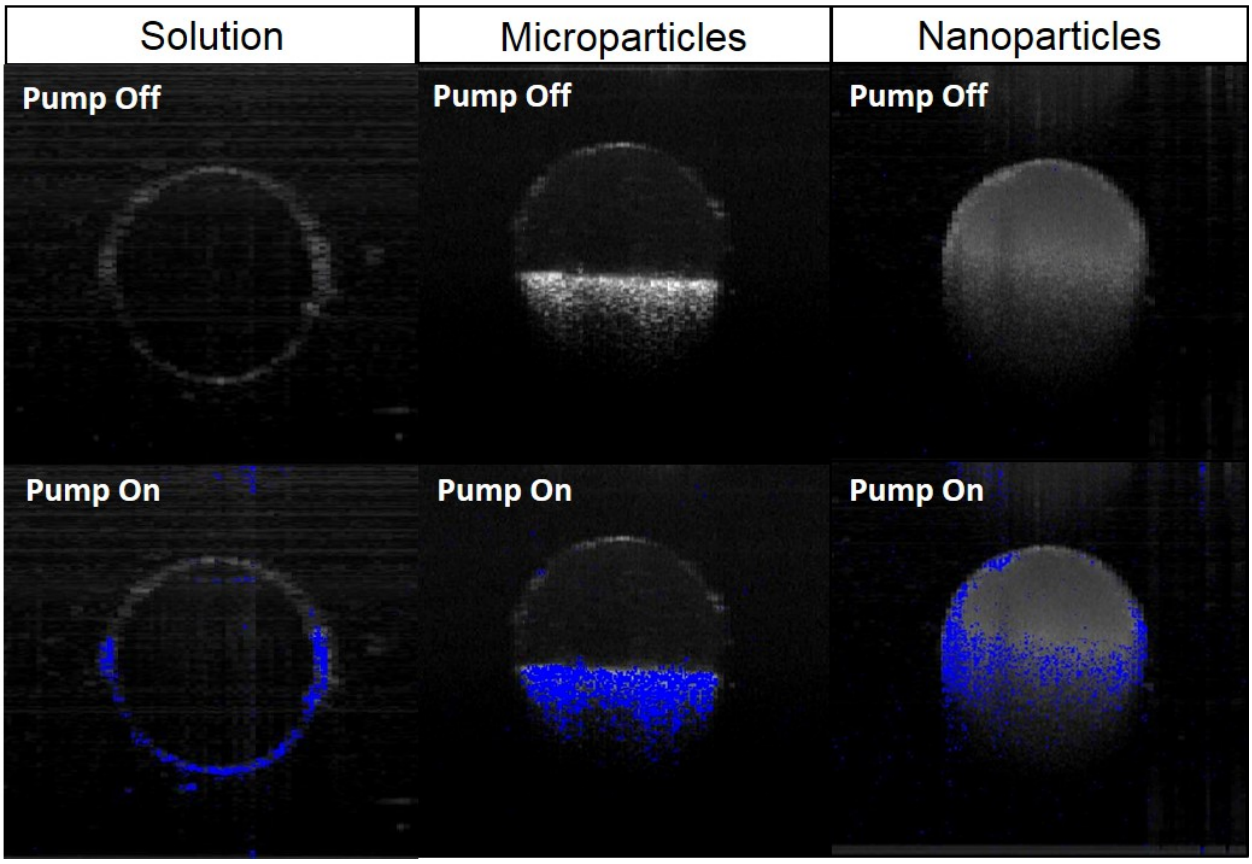

Figure 2.13: PDMS microchannels of 500 μm diameter, were loaded with MB solution, MB microparticles and MB nanoparticles. Top row shows PPOCT B-Scan acquired with pump light source off. On the Bottom row, Pump was activated and MB molecules, either in solution or loaded inside of the polymeric spheres, were localized on the PPOCT B-Scan (blue).

can be primarily controlled by particle size, the contrast-to-noise-ratio can be optimized by the photophysics and the concentration of the contrast agents. Methylene blue was selected as our contrast agent due to its low cytotoxicity (FDA approved), and its ground and triplet state absorption peaks that match available pump and probe/OCT light sources. The functionality of methylene blue as a PPOCT contrast agent is highly affected by its molecular state (monomer vs dimer) at the imaging site. Since our PPOCT system is equipped with a 663 nm pump light source, MB in the monomeric form is favorable as its ground state absorption peak is located at the same corresponding wavelength. The co-presence of MB in monomeric and dimeric forms, described as the D/M ratio herein, can be primarily controlled by MB concentration [45]. Generally, as the con-

centration of MB in free solution increases (from 20 μM to 200 μM), the D/M ratio increases (Fig. 2.5). This is likely because the spatial distances among MB molecules were relatively decreased and, thus increasing a probability for MB to form dimers or aggregates at higher concentration. Similar results were also observed when MB was encapsulated within PLGA particles. Within the PLGA polymer matrix, the distance among MB molecules are further reduced. As expected, at the same MB concentration, the D/M ratio of encapsulated MB was found to be higher compared to free MB (Fig. 2.6). In addition, negatively charged COOH-PLGA polymer used in this study could possibly further enhance MB dimerization as it can attract MB (positively charge in solution) binding to the polymer surface [14, 38, 44].

Ground state optical properties of MB particles were characterized in order to find an optimal D/M ratio that optimizes MB ground state absorption of the pump light source (660 nm) and provides the highest pump-probe signal intensity. The desired D/M ratio within the particles can be obtained by controlling the amount of MB encapsulated in the particles, namely MB encapsulation efficiency. Our experiment has shown that the encapsulation efficiency can be modulated by the pH of water phase used during the emulsification process. As the water phase pH increases, the encapsulation efficiency was found to increase linearly from pH 4 to pH 8.4 (Fig. 2.8). This could be partly because the level of MB dimerization was enhanced in the alkaline solution [50, 56]. The formation of MB aggregates may delay and hinder MB molecule clusters from leaking out of the polymer matrix/shell during the fabrication process, resulting in the higher encapsulation efficiency at a higher pH. In addition, it is possible that the increase of water phase pH changes the charge distribution/polarity at the water phase-PLGA chain border, which slows down the MB diffusion to the outer phase [57, 58]. Microparticles synthesized using a pH of 8.4, provided the best encapsulation efficiency (82.6%) and the highest CNR (5.86). Once the optimal fabrication parameters were determined for microparticles, MB-PLGA nanospheres were prepared following the same protocol with the only difference being the shear stress/time applied to the emulsion.

PLGA particles are biodegradable, thus are expected to release drugs in physiological conditions over time. Monomer ratio (lactic acid:glycolic acid) and polymer molecular weights are

common PLGA properties that are varied to achieve desired drug release kinetics and profiles for specific applications. For our PPOCT imaging, the expected average procedural and imaging times are approximately two hours. As shown in Fig. 2.9, 50:50 PLGA nanoparticles loaded with 2.83 mM released 81% of encapsulated MB in the first 2 hours of incubation at 37°C, compared to 11% of MB from 50:50 PLGA microparticles during the same time frame. The faster release profiles observed in nanoparticles could be explained by a greater surface-to-volume ratio compared to microparticles, and the overall location of encapsulated MB molecules which tend to concentrate relatively close to the sphere surface. By fabricating the nanoparticles using PLGA having a higher molecular weight and a higher lactic/glycolic ratio (75:25), the MB release was shown to be significantly reduced particularly during the procedural time frame. This result agrees with previous works reporting that a slower release profile is associated with PLGA polymer with a higher lactic acid to glycolic acid ratio [47, 51]. Although some of MB might be released during in-vivo imaging procedures, our in-vitro studies (Fig. 2.9) suggest that the MB release from 50:50 PLGA microspheres and 75:25 PLGA nanospheres during this time window should not compromise the contrast imaging sensitivity.

In addition to enabling specific target localization and controllable imaging signal contrast, the carrier system also provides an environment where the physical distribution and the state of MB molecules are preserved, unlike the free MB that is undetermined once it enters the blood circulation. The susceptibility of enzymatic reduction is one of methylene blue biggest drawbacks for in-vivo therapeutic and molecular imaging applications. In circulation, MB is reduced by either NADH/NADPH dehydrogenases or enzyme reductase in red blood cells and peripheral cells to colorless leukomethylene blue (LMB) [24, 25, 26], which changes its spectral properties to be invisible for the PPOCT imaging system. By encapsulating MB into PLGA particles, MB was protected from enzymatic interactions. Specifically, 95% of MB encapsulated within microparticles and 88% of MB encapsulated within nanoparticles remained in their native states after 30 min of enzymatic exposure (Fig. 2.10). These results indicate that a majority of MB remains immobilized within the PLGA matrix during the enzymatic exposure. The slight decrease of intensity from

the encapsulated MB could be attributed to the reduction of MB molecules bound at the particle surface. This result demonstrates that a protective environment formed by the PLGA matrix successfully prevents large enzymatic molecules to penetrate and interact with the encapsulated MB. Thus, MB-PLGA provides an extended circulation lifetime for MB, which in turn reduces the need of high doses and potentially minimizes associated cytotoxicity.

To create an image from PPOCT with MB-PLGA contrasts, the pump-probe signal was recorded by pumping MB molecules into the excited state using a modulated light source centered at 660 nm and sequentially measuring transient absorption of probe light source centered at 830 nm. OCT M-scans were collected and processed in the traditional way as previously described [7, 11]. The processed OCT M-scans were Fourier transformed along the time dimension and filtered around the pump modulation frequency leading to the reconstruction of PPOCT images. Upon 660 nm excitation, MB molecules generate reactive species which can deconstruct and compromise the integrity of proximal tissues its unique properties that has been widely employed as a photodynamic therapy drug for cancer. However, this radical generation is unfavorable in diagnostic applications and non-photodynamic treatments. Figure 2.11 shows that the local release of radical species generated by excited MB was significantly reduced when MB was encapsulated within the PLGA particles. This reduction could be contributed to several factors including the formation of MB dimers (Fig. 2.6), a longer diffusion path within the PLGA matrix, and a quenching of MB excited states. Since MB dimers have a different absorption peak (at 600 nm, compared to 660 nm for MB monomers), they do not produce $^1O_2$ upon 660 nm irradiation. Also, there are two photochemical pathways (type I and type II) that are involved in the photoinduced generation of reactive species [14, 43]. In the type I mechanism, excited MB transfers electrons to biomolecules and forms several different radical species. In the type II pathway, excited MB transfers energy to surrounding oxygen molecules and generates $^1O_2$. Type II is generally accepted as a primary pathway that is responsible for photobiological activities while type I is a secondary mechanism [59]. MB dimers have been previously shown to shift the photochemical pathways for MB from type II to type I, resulting in the decrease in $^1O_2$ formation [14, 44]. Lastly, since $^1O_2$ molecules exist just for a

few microseconds, a longer diffusion time could mean that $^1O_2$ generated by MB inside of the sphere recovers to the stable form $^3O_2$ before being able to leave the particle. This result shows that MB-PLGA particles can hinder local sequestration of $^1O_2$ and suppressing an adverse effect that associates with MB utilization. Although, MB dimers seem to prevent the generation of $^1O_2$, they dont contribute to the generation of Pump-Probe contrast. Therefore, a low D/M ratio is still preferred inside the PLGA particles.

Since our PPOCT imaging setup is sensitive to variations in MB concentration, specifically to the ratio of MB monomers/dimers and the enzymatic reduction of MB into Leuco-MB, having the capability to control the distribution of MB molecules inside our PLGA spheres provide an apparent improvement compared to free solutions of MB as contrast agent. In addition, the inherent backscattering produced by the PLGA shells enhances the OCT signal. Thus, using MB-loaded PLGA particles provides both enhancement of morphological imaging and molecular contrast.

3. FUNCTIONALIZATION OF MB-PLGA PARTICLES TO TARGET ATHEROSCLEROTIC PLAQUE BIOMARKERS

3.1 Introduction

Atherosclerosis is the main underlying cause of the majority of cardiovascular diseases (CVDs), and the principal source of morbidity and mortality in the US [60]. Atherosclerosis is a condition in which plaque accumulates on the inner wall of arteries. Plaque accumulation can partially or totally block the bloods flow, or erode and rupture the artery leading to thrombosis, myocardial infarction or stroke [61]. Imaging techniques such as Intravascular Ultrasound (IVUS) and Optical Coherence Tomography (OCT) have emerged as intravascular diagnostic tools offering anatomic assessments of the atherosclerotic plaque. A much higher axial and lateral resolution and faster data acquisition, makes OCT more suitable for assessing coronary vessels from an anatomic standpoint compared to IVUS [62]. OCT can be used to acquire high-resolution morphological images of atherosclerotic plaques enabling identification of biomarkers including fibrous tissue thickness, area of necrotic core and calcifications. However, due to the high speckle and low contrast on OCT signal, evaluation of atherosclerotic plaque images can be very challenging even for expert readers, frequently leading to plaque misclassification [63].

Simultaneous structural and molecular imaging are critical particularly for the diagnosis of complex diseases. In acute coronary events, for instance, research has demonstrated that imaging techniques providing anatomical structure of blood vessel alone insufficiently predicts patient outcome. Because a narrowed lumen is not always a predicting sign for high-risk vulnerable plaque [64], additional information on molecular details has been demonstrated to be valuable for plaque classification, predicting lesion severity and future risk of acute coronary events. Studies from our group have shown that by integrating endogenous fluorescence lifetime imaging microscopy (FLIM) technique along with OCT, both morphological and biochemical compositions of lipid and collagen on atherosclerotic lesions can be simultaneously derived [64]. In parallel to multimodal

strategies, this research work seeks to develop targeted contrast agents that complementarily aids intravascular OCT imaging of atherosclerotic plaques.

Surface functionalization of the MB-PLGA particles developed in Chapter 2 can enable targeting specific molecular biomarkers of atherogenic processes, such as inflamed endothelium and macrophage deposits (foam cells or apoptotic macrophages). This work was focused on VCAM-1, an endothelial adhesion molecule involved in the recruitment of monocytes and their internalization into the arterial intima layer.

The properties of MB-PLGA particles as targeted contrast agents for PPOCT imaging and their tissue permeability were evaluated in cell-free environment, tissue phantoms and human postmortem artery. Molecular details provided by MB-PLGA were verified by means of tissue histopathological evaluation.

3.2 Materials and Methods

3.2.1 Materials

Dulbeccos Phosphate Buffered Saline (DPBS) and N-(3-Dimethylaminopropyl)-N-ethyl carbodiimide (EDAC) were purchased from Sigma-Aldrich. DiO and NeutrAvidin protein were acquired from Thermo-Fisher. Biotinylated vascular cell adhesion molecule 1 (VCAM-1) antibodies were purchased from Abcam. Sialyl Lea-PAA-biotin (SLea) was acquired from GlycoTech. Cutaneous lymphocyte-associated antigen (CLA-PE) was obtained from Miltenyi Biotec. Fluorescein rabbit antimouse IgG-1 was purchased from Jackson Immunoresearch. MESF calibration bead was purchased from Bangslab. IL-1β was acquired from Fitzgerald. All reagent grade organic solvents were purchased from VWR.

3.2.2 Post Mortem Human Coronary Sections

Postmortem unfixed coronary segments from human hearts were obtained from non-specific adult autopsy cases. The artery sections were harvested, immediately stored in DPBS at 4°C and used within 48 hours. Arterial segments were handled in accordance to protocols approved by the Texas A&M University Institutional Review Board (IRB).

3.2.3 Endothelium Permeability Test

Intact coronary segments were treated with fluorescent DiO microparticles (1x10^8 µp/mL) and DiD nanoparticles (1x10^{12} np/mL) suspended in warm DPBS (37°C) inside a 15 mL centrifuge tube. DiO and DiD particles were fabricated using the same methods described in chapter 2, with similar average diameters to MB micro and nanoparticles. Artery sections were incubated at 37°C for 20 minutes. After incubation, tissues were fixed in 10% formalin for 48 hours, and prepared for cryopreservation by suspending in a 30% sucrose solution overnight. Coronary segments were then embedded in an optimal cutting temperature compound and rapidly frozen using liquid nitrogen. Cryo-sectioning and slide preparation were performed by the histopathology lab at the Texas A&M College of Veterinary Medicine. Histology sections were then analyzed by confocal fluorescence microscopy at emission wavelengths of 501 nm for DiO microparticles and 665 nm for DiD nanospheres.

Additionally, an artery segment was cut along the longitudinal direction of the vessel and prepared for PPOCT imaging. The artery was treated with a suspension of MB microparticles suspended in warm DPBS (37°C), incubated for 10 minutes and imaged. In order to compare the penetration of MB micro and nanoparticles, the same arterial section was rinsed with DPBS to remove microparticles, and treated this time with a suspension of MB nanoparticles. After 10 minutes of incubation, the artery was imaged with our PPOCT system.

3.2.4 Functionalization of PLGA Particles for Atherosclerotic Plaque Targeting

PLGA particles were labeled with targeting ligands via EDAC-carbodiimide and avidin-biotin linkages as previously described [32]. Briefly, carboxylated PLGA spheres were initially modified with NeutrAvidin proteins in EDAC and MES buffer. Subsequently, biotinylated human VCAM-1 antibody was added to PLGA micro and nanoparticles. Functionalized particles were washed in DPBS, collected by centrifugation, and stored at 4°C in the dark until use. The coverage density of VCAM-1 antibodies on the microparticle surface was measured by flow cytometry (FACSCalibur, Becton, Dickinson and Company). Microparticles were stained with FITC-labeled rabbit anti-

Mouse IgG (H+L) secondary antibodies. Non-stained aVCAM-1 microparticles, avidin-coated microparticles stained with the secondary antibodies and aVCAM-1 microparticles stained with isotype controls were used as controls. Fluorescence intensities obtained from flow cytometry were converted to ligand surface density via a calibration curve relating the fluorescence peaks of Quantum Standard Beads to their molecules of equivalent soluble fluorochrome (MESF); fluorophore to protein (F/P) ratio between the primary antibody (FITC) to protein was assumed to be 1:1.

Similarly, functionalization of PLGA nanoparticles was evaluated by an ELISA assay. Avidin conjugated PLGA micro and nanoparticles were incubated with biotin-labeled horseradish peroxidase (B-HRP) for 30 min. Particles were then washed with PBS to remove unbounded BHRP and then transferred into an opaque 96-well plate. Amplex Red fluorescent peroxidase was added to samples, allowing for a 10-min reaction [55]. The fluorescent intensity of untreated (control) and Amplex Red treated micro and nanoparticles was measured using a microplate reader (Synergy HTX, BioTek). The surface area of both micro and nanospheres was fixed in order to compare their surface ligand density.

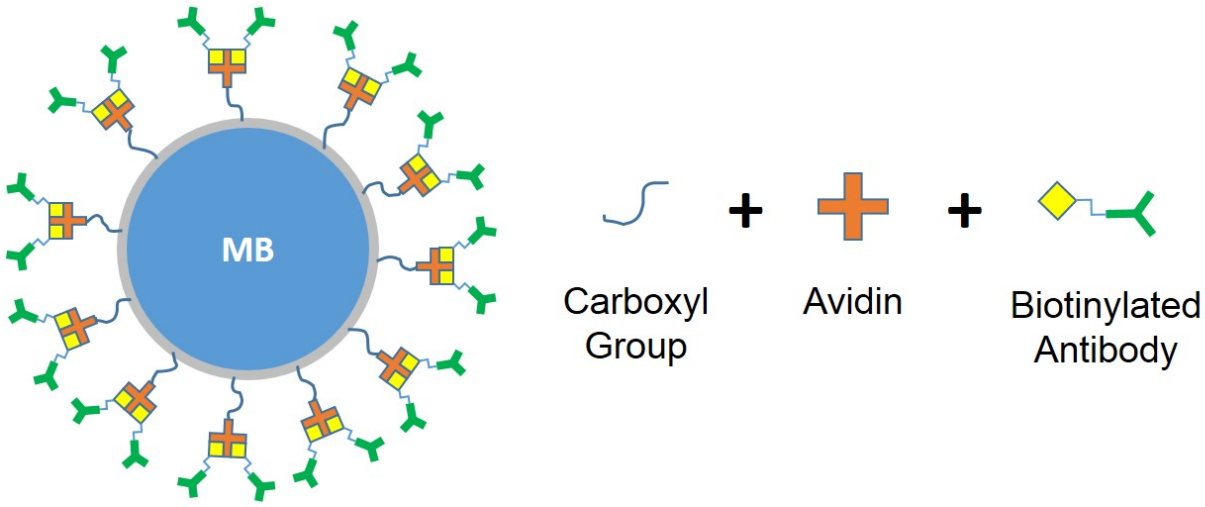

Figure 3.1: Functionalization diagram of PLGA particle surface with biotinylated antibodies.

3.2.5 MB Microparticles Targeted to Ex-Vivo Human Artery Sections

Human arterial segments were cut along the longitudinal direction of the vessel, hydrated with warm DPBS (37°C) and placed inside a custom-made parallel flow chamber with the lumen facing up. A custom-made flow chamber of 1 mm in height by 5 mm in width, was designed to hold an artery section and allow a laminar flow on top of its lumen (Fig. 3.2). Tissues were placed in the chamber, treated with either MB solution (50 µg/mL), a-VCAM1 functionalized MB-PLGA microparticles (1x10^7 p/mL) or uncoated MB microparticles (1x10^7 p/mL) suspended in warm DPBS, and incubated at 37°C for 20 minutes. Arterial segments incubated with MB solution and non-targeted MB particles were used as a control.

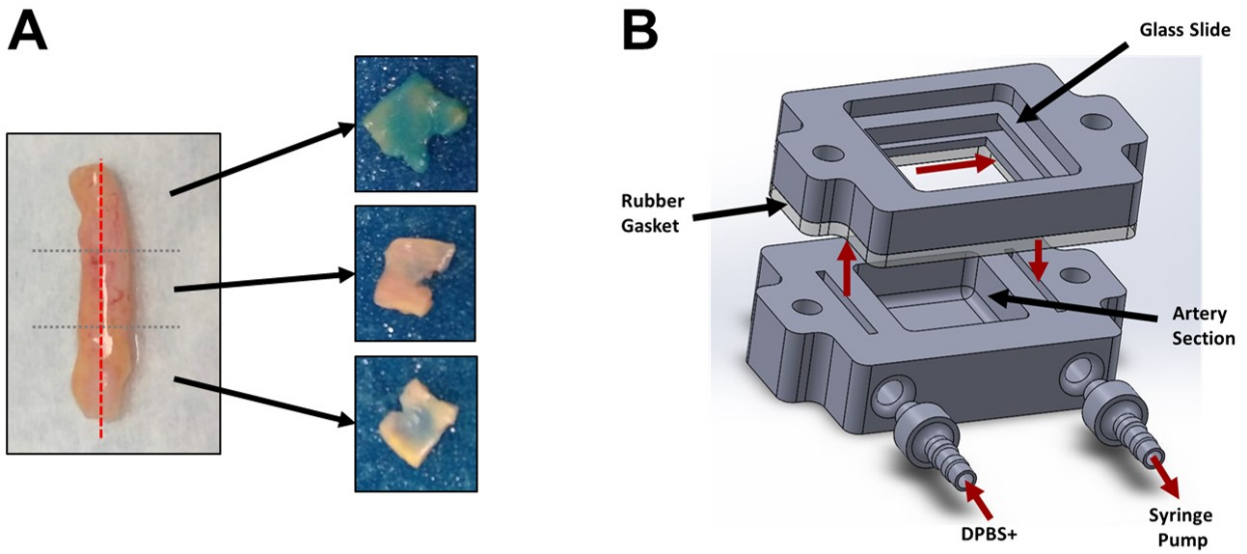

Figure 3.2: (A) Post-mortem human artery divided in 3 sections and treated with either MB solution (75 µg/mL), uncoated MB microparticles (1x10^7 p/mL) or a-VCAM1 functionalized MB-PLGA microparticles (1x10^7 p/mL) suspended in warm DPBS+. (B) 3D rendering of the custom-made flow chamber designed to hold human arterial sections and generate laminar flow over the artery lumen.

After incubation, arteries were washed with DPBS (37°C) under flow (wall shear rate = 100 s^{-1}) for 5 minutes to remove unbounded particles. The flow chamber lid was removed, the excess of DPBS was carefully removed, and the arteries were imaged using the previously described

PPOCT system. After imaging, the arterial segments were fixed in formalin sent to a pathologist who prepared tissue slides. Histopathological evaluation of digitized artery segments was performed to confirm specificity of aVCAM-1 functionalized microparticles and evaluate PPOCT imaging efficiency to locate MB-based contrast agents.

3.3 Results

3.3.1 Endothelium Permeability Test

Permeability of non-functionalized DiO-PLGA spherical microparticles and DiD-PLGA nanoparticles was studied in post-mortem human artery sections. Confocal fluorescence images show that permeability of PLGA particles through the arterial endothelium was mainly size-dependent (Fig. 3.3). While DiO microspheres (2-4 μm) mostly remained at the superficial layer (Fig. 3.3.A), DiD nanospheres (80-120 nm) could enter into the deeper layers (intima, media and adventitia) (Fig. 3.3.B).

PPOCT images of an arterial section treated sequentially with MB micro and nanoparticles also demonstrated a size-dependent PLGA particle permeability. Figure 3.3.E shows that MB microparticles remained mainly at the surface of the artery. On the other hand, the PPOCT image of the same artery section treated with MB nanoparticles registered pump-probe signal at least two tissue layers deeper compared to microparticles (Fig. 3.3.F).

3.3.2 Conjugation of PLGA Particles to Vascular Endothelium Receptors

Active targeting of the inflamed vascular endhothelium was enabled by the conjugation of functionalized biotin-VCAM-1 antibodies on MB-PLGA micro and nanospheres. A flow cytometer shift of the particles stained with FITC-secondary antibody confirmed aVCAM-1 immobilized on the microparticle surface (Fig. 3.4). Human aVCAM-1 ligands were immobilized on MB microparticles with a site density of approximate 2959.76 sites/μm^2.

Functionalization of PLGA-MB micro and nanoparticles was analyzed by an ELISA essay. The fluorescence intensity generated by the secondary antibody attached to both micro and nanoparticles suggest a 2-fold increase of the site density for nanosphered compared to microparticles (Fig.

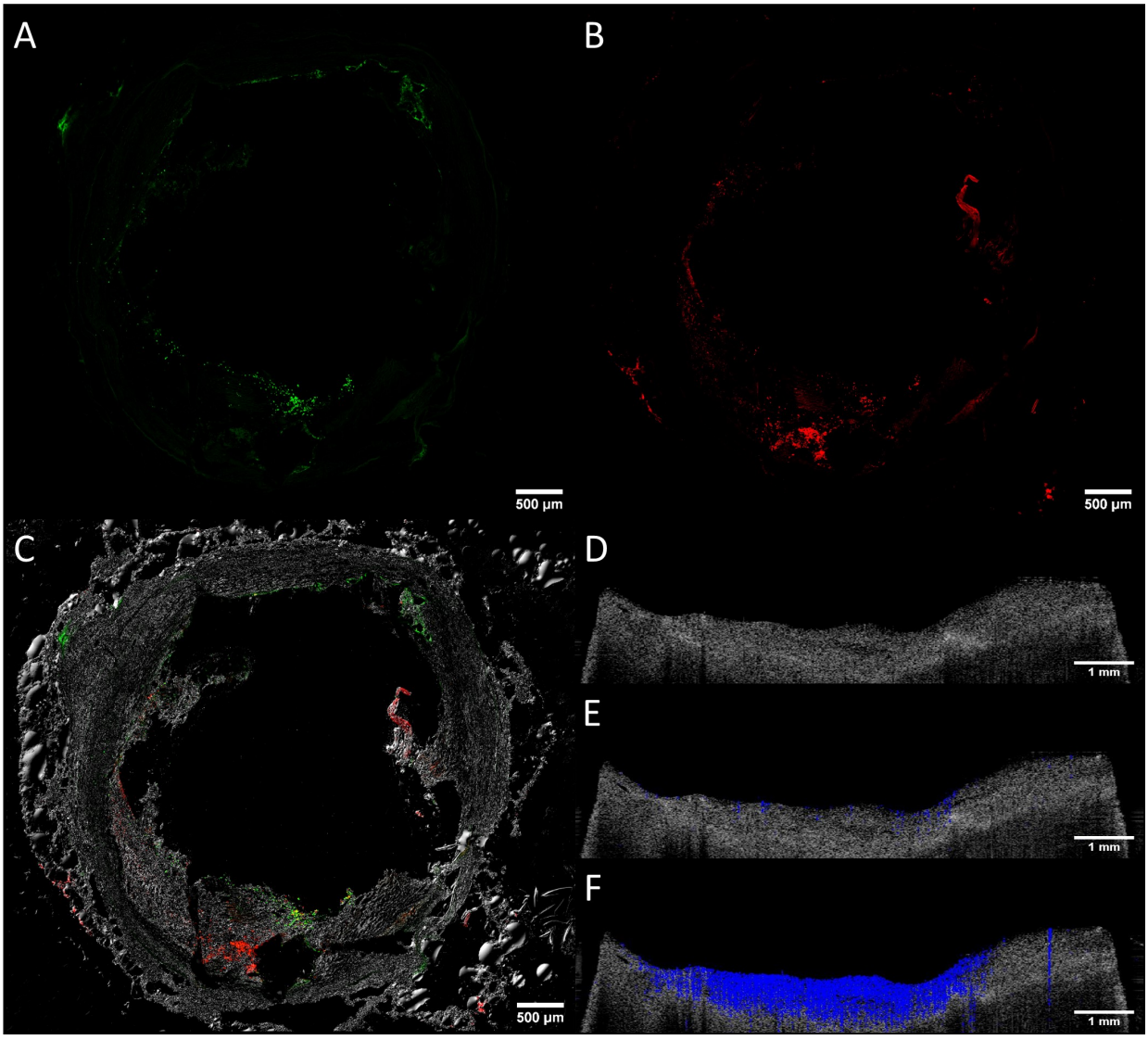

Figure 3.3: Confocal fluorescence microscope images of post-mortem human artery sections incubated with (A) DiO-PLGA microparticles, (B) DiD nanoparticles and (C) bright field overlaid. PPOCT images of an artery section (D) untreated, (E) MB microparticles and (F) MB nanoparticles.

3.4).

3.3.3 Ex-vivo Imaging of Atherosclerotic Human Arteries.

To further study the feasibility of MB-PLGA particles as targeted molecular contrast agents for PPOCT, an ex-vivo experiment was designed to validate the targeting of aVCAM1 functionalized MB particles and their attachment stability under flow conditions. Figure 3.5 shows PPOCT images

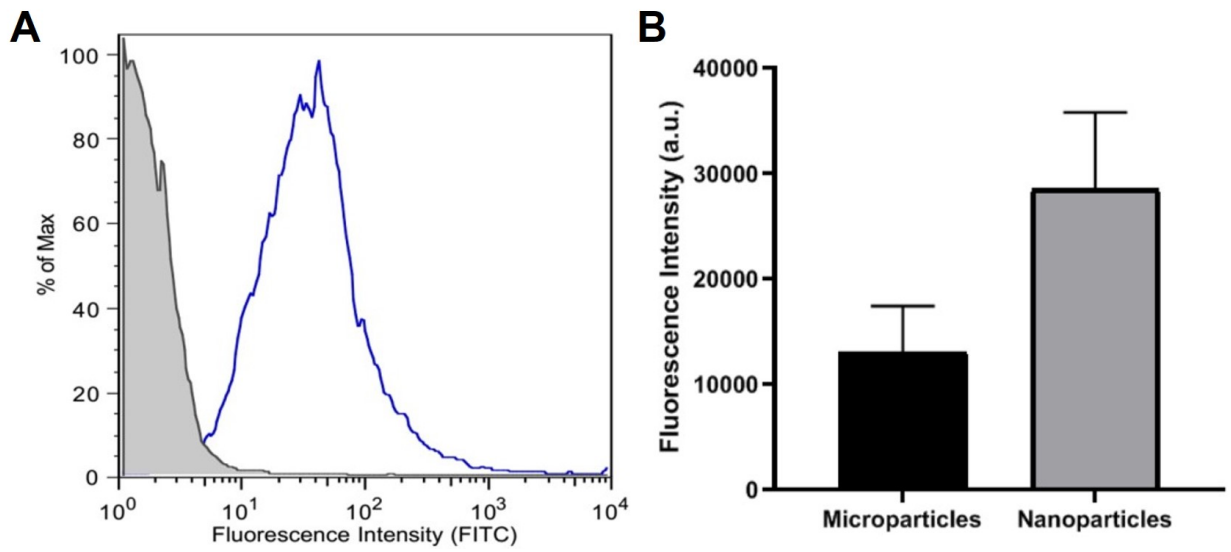

Figure 3.4: Flow cytometry histogram of aVCAM-1 MB-PLGA microparticles labeled with a FITC-secondary antibody (blue) and uncoated MB-PLGA microparticles (gray). Fluorescence Intensity of an ELISA essay of functionalized micro and nanoparticles.

of three artery sections treated with either a 75 µg/mL MB solution, uncoated MB microparticles, or aVCAM-1 functionalized MB microparticles. Histological analysis of artery sections treated with functionalized MB-PLGA particles, demonstrated specific binding of microparticles to tissue sites rich in macrophages, which are sign and cause of an inflammatory process.

PPOCT B-Scans were processed in MATLAB as described in Chapter 2. 3D rendering of PPOCT M-Scans was performed by using a 3D toolbox in ImageJ. Figure 3.6 illustrates the distribution of aVCAM-1 functionalized MB microparticle on the arterial endothelium.

3.4 Discussion

PLGA-based carriers have been broadly used as contrast agents and therapeutics in the clinics due to their safety and simple fabrication process [32]. Herein, PLGA-based contrast agents were developed for PPOCT imaging of atherosclerotic lesions. The contrast agents were designed to enhance morphological imaging and provide molecular details at the arterial surface and within the atherosclerotic plaque, which are essential for predicting the plaque vulnerability. Of multiple physiological processes regulated by the endothelium, inflammation is of particular interest

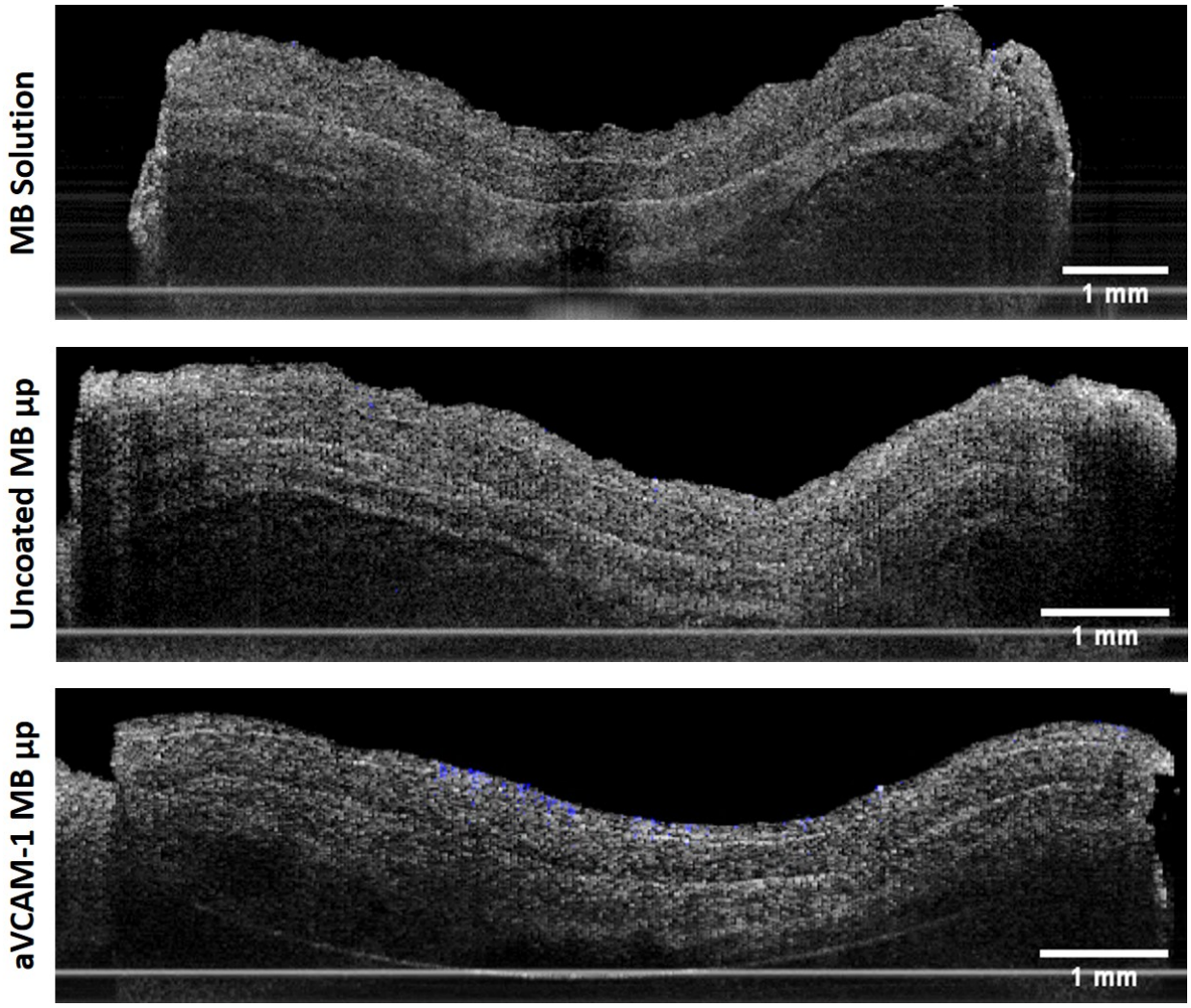

Figure 3.5: PPOCT (blue) overlaid on top of OCT (gray) images of ex vivo human coronary artery sections incubated with MB solution (top), uncoated MB microparticles (middle), or aVCAM-1 coated MB microparticles (bottom).

for vascular targeting due to its known involvement in the pathogenesis of atherosclerosis [65]. Molecules such as selectins, ICAM-1 and VCAM-1 are primarily expressed by endothelial cells during an inflammatory response to help recruit leukocytes to the vascular wall. These biological receptors represent a hallmark of inflammation response commonly associated to atherogenic processes.

Although vascular endothelial integrity could be compromised in ex-vivo tissues, our permeability experiments presented a similar trend to findings observed from in-vivo experiments per-

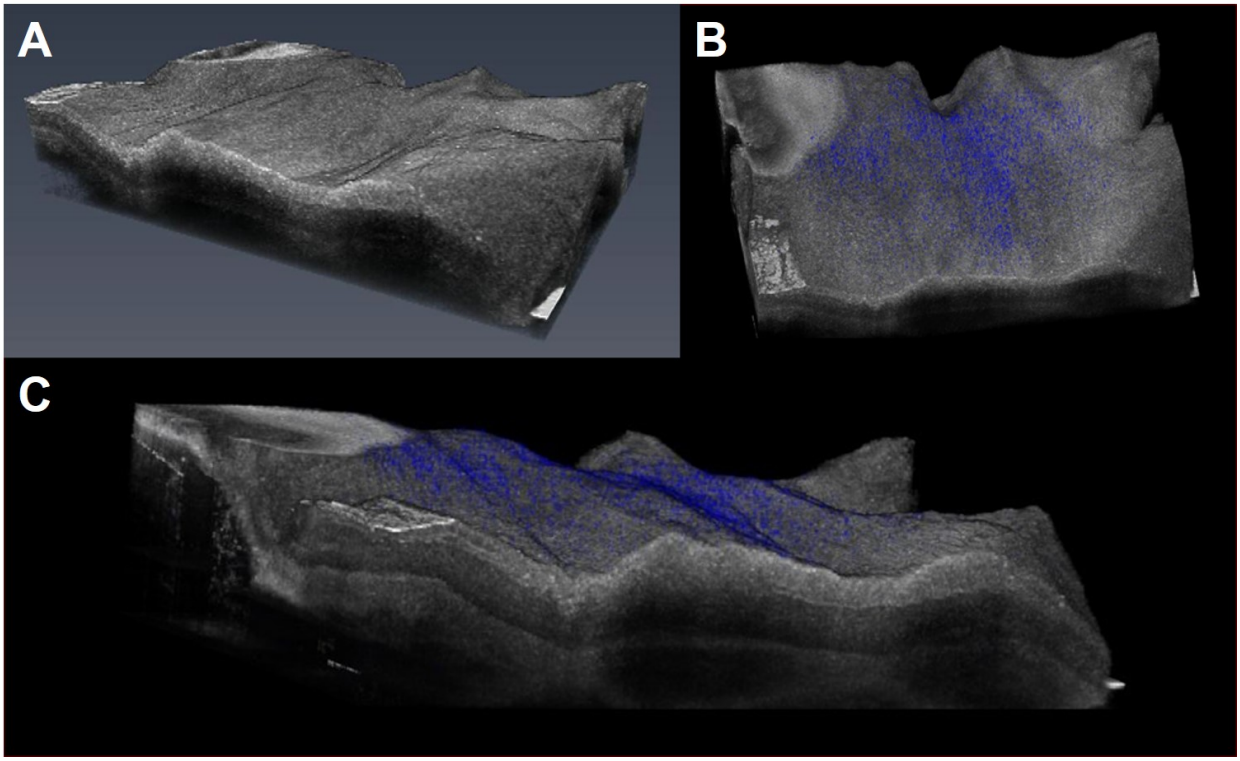

Figure 3.6: 3D rendering of a PPOCT volume acquired by imaging a post-mortem human artery section treated with aVCAM-1 functionalized microparticles. (A) 3D-OCT, (B) Top-view PPOCT, (C) Cross-section PPOCT.

formed at several other research works [34, 66]. Since the particle permeability experiment was performed under static conditions, penetration of PLGA particles through the arterial endothelium was mainly determined by sphere average diameter. Endothelial cell junction gaps in atherosclerotic plaques might be big enough to let nanoparticles permeate much deeper than microspheres, making them a better approach for foam cells targeting and imaging [34, 35]. Higher permeability of MB nanoparticles under in-vivo pressure and flow conditions could be expected, making these contrast agents suitable for imaging and characterization of plaque biomarkers in deeper tissue layers. Overall, the permeability experiments demonstrated the potential of PLGA particles to penetrate into human atherosclerotic plaques and localize relevant pathological biomarkers.

For simplicity, only one cell adhesion molecule (VCAM-1) was used to conjugate MB micro and nanoparticles. However, the methodology presented in this chapter can be used to functionalize

PLGA spheres with other biotinylated molecules/antibodies to target/image other critical biomarkers in atherosclerosis such as CD36, a membrane protein related to macrophage foam cell formation. These targeted PLGA platforms could therefore enable the characterization of pathogenic processes by investigating molecular activity and receptor expression at the vascular endothelium.

Ex-vivo experiments confirmed the specific binding of functionalized MB microparticles to human vascular endothelium inflammatory receptors. A static incubation of aVCAM-1 microparticles was selected due to the dimensions of the custom-made flow chamber, since a big number of spheres would have been needed to run a flow experiment at the rate and particle concentration desired. To minimize the effect of non-specific binding of PLGA particles, artery sections were washed under flow at 100 s^{-1} with DPBS+. PPOCT images demonstrates the potential of these targeted contrast agents.

Finally, the FDA approval of both MB and PLGA could make clinical translation much easier, which means that not only researchers in the biomedical field but also physicians could be provided with targeted molecular contrast tools for PPOCT imaging that allow them to characterize different stages of atherosclerotic disease, improving plaque stability diagnosis. In addition, a better understanding of the atherosclerotic pathways, and monitoring these molecular tags before, during, and after administration of current and exploratory treatments could accelerate the development of more accurate drugs and curative therapies.

4. MULTISTAGE DELIVERY SYSTEM

4.1 Introduction

Targeted drug delivery platforms have been investigated with promising results on enhancing the effectiveness of treatments, reducing the drug dosage required to treat complex conditions and therefore minimizing adverse effects on healthy tissues. Researchers have demonstrated that physicochemical properties of drug carriers significantly influence the efficiency of delivery systems. Specifically, micron-sized particles favor localization to the inflamed vascular wall in atherosclerosis-flow environments [55].

Current treatments for atherosclerosis are mainly based on surgical interventions and statin therapy. These strategies do not prevent recurrence, require long recovery times and are commonly associated with side effects. In recent years, vascular targeted nanoparticles have been investigated as reliable therapeutic carriers due their ability to permeate into deeper tissues, especially on health conditions that compromise the vascular endothelium such as cancer and atherosclerosis [34, 67]. However, nanoparticle location to the vascular wall is often limited in dense blood flows, resulting in accumulation in filtering organs and non-targeted tissues, which has limited their clinical translation [68].

The need for more effective drug delivery carriers that allow the reduction of drug dosage and the off-site secondary effects, is critical to reducing healthcare costs, improving outcomes and recovery times for patients worldwide. Since microparticles (2-5 μm) have demonstrated significantly superior margination in human blood flows, several multistage delivery systems (MDS) have been developed in recent years to improve the delivery of nanoparticles to the vascular wall [69, 70]. To our knowledge, most current multistage delivery strategies make use of non-degradable polymers for their encapsulated nanocarriers.

In this work, a biodegradable multistage delivery system (MDS) based on Poly-lactic-co-glycolic-acid (PLGA), has been developed to improve the overall vascular-targeting efficacy, both

blood flow localization and tissue penetration, for atherosclerosis imaging and treatment. PLGA has FDA approval and have been used in the clinics. The fabrication process for PLGA is also simple, scalable and can be optimized for controlled payload release. In addition, the tunable biodegradability and capability for PLGA to encapsulate hydrophilic and hydrophobic molecules, as well as protein drugs, allow various compounds to be simultaneously delivered in a controlled manner. This PLGA-based MDS consists of two stages: 1) a micron-sized outer shell and 2) encapsulated nanoparticles, aiming to achieve both effective margination and intracellular entry. MDS is a modular platform, consisting of a microsphere outer shell primary stage and an encapsulated nanosphere secondary stage carrying a payload of interest.

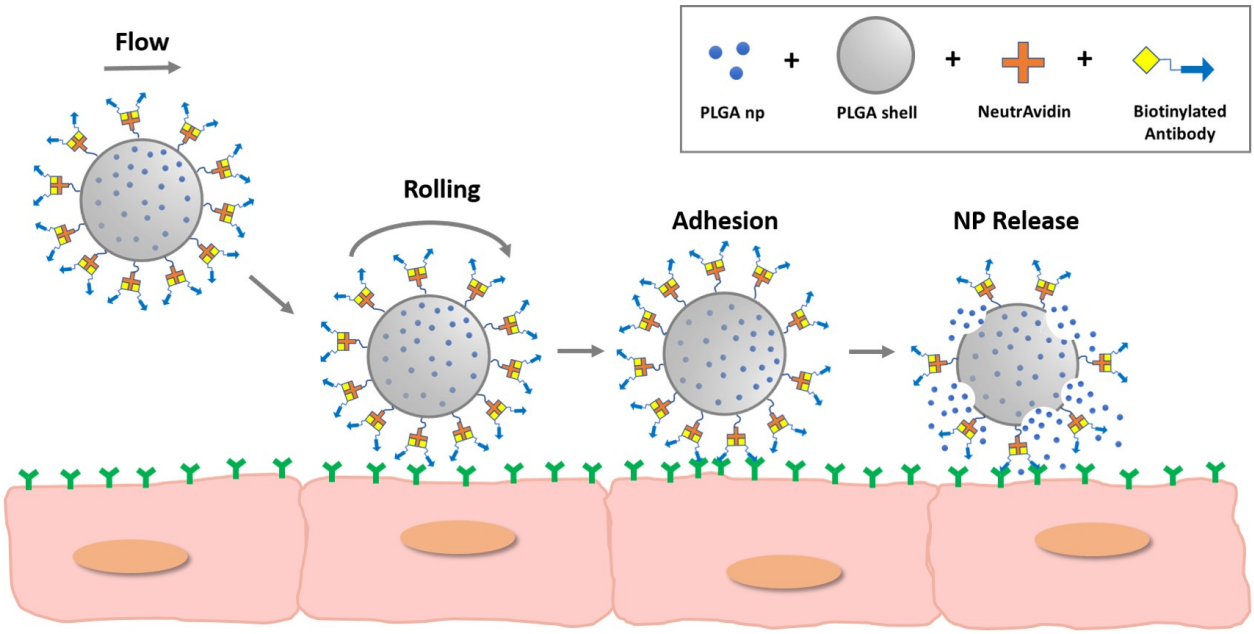

Figure 4.1: Schematic of the MDS drug-delivery strategy as a vascular-targeted microcarrier for PLGA nanoparticles.

4.2 Materials and Methods

4.2.1 Materials

Poly Lactic-co-Glycolic Acid (50:50 and 75:25 PLGA) were acquired from Evonik Industries. Poly Ethylene-Maleic Acid (PEMA), Poly Vinyl Alcohol (PVA), Chitosan, Dulbeccos Phosphate Buffered Saline (DPBS) and N-(3-Dimethylaminopropyl)-N-ethyl carbodiimide (EDAC) were purchased from Sigma-Aldrich. DiO and NeutrAvidin protein were acquired from Thermo-Fisher. Methylene Blue (MB) was obtained from Fisher Scientific. Biotinylated vascular cell adhesion molecule 1 (VCAM-1) antibodies were purchased from LSBio. Sialyl Lea-PAA-biotin (SLea) was acquired from GlycoTech. Cutaneous lymphocyte-associated antigen (CLA-PE) was obtained from Miltenyi Biotec. Fluorescein rabbit antimouse IgG-1 was purchased from Jackson Immunoresearch. MESF calibration bead was purchased from Bangslab. IL-1β was acquired from Fitzgerald. HUVEC cells and EGM-2 Medium were obtained from Lonza. All reagent grade organic solvents were purchased from VWR.

4.2.2 Fabrication of Chitosan-Coated PLGA Nanospheres

DiO and MB PLGA nanoparticles were prepared by an oil-in-water (O/W) emulsion solvent evaporation method [36, 37]. Briefly, an oil phase was prepared by dissolving 0.5 mg of selected chromophore (DiO or MB) and 20 mg of PLGA polymer (75:25) in 2 mL dichloromethane (DCM). Then, the oil phase was added dropwise into 10 mL of continuous water phase containing polyvinyl alcohol (PVA) and poly-ethylene-maleic Acid (PEMA) dissolved in DI water. During the emulsification process, the oil phase was broken into small nanodroplets by high energy shear stress produced by either a homogenizer (FSH 125, Fisherbrand) or a 20 kHz sonicator tip (Q125, QSonica). To ensure complete evaporation of organic solvent and solidification of nanoparticles, the emulsion mixture was stirred under a fume hood for 3 hours. To remove the remaining surfactant in water phase, spheres were washed in DI water and collected via ultracentrifugation. Serial centrifugation was used to narrow down size distribution.

Subsequently, the formed PLGA nanoparticles containing either MB or DiO were coated chi-

tosan to protect their integrity during the following emulsification process. Briefly, a fresh chitosan solution was prepared by dissolving chitosan in a sodium acetate buffer (pH 4.5). Nanoparticles were suspended in a 0.1 mg/mL chitosan solution to ensure a homogenous surface coating. After an overnight incubation particles were washed and recovered via ultracentrifugation.

Particles size distribution and concentration were determined using a nanoparticle tracking analysis system (NanoSight LM10, Malvern Instruments). Nanoparticle surface charge was characterized by zeta potential (Zetasizer Nanoseries, Malvern Instruments). Morphology of PLGA particles was verified by scanning electron microscopy (SEM Neoscope JCM-5000, Nikon). Encapsulation efficiency was determined by measuring light absorption for MB or DiO nanoparticles at 484 and 665 nm, respectively, and comparing against calibration solutions of known concentrations, using a microplate reader (Synergy HTX, BioTek). Encapsulation efficiency was defined as the ratio of total MB or DiO obtained from dissolved particles divided by the initial amount of MB or DiO used during the particle fabrication process. The release of MB and DiO from nanoparticles was determined by incubating particles in phosphate buffered saline at 37°C and periodically measuring the light absorption of the released MB or DiO suspended in the supernatant using the microplate reader.

4.2.3 Fabrication of PLGA-Based MDS

MDS microcapsules were prepared by a water-in-oil-in-water (W/O/W) emulsion solvent evaporation method (Figure 4.2). Briefly, chitosan coated PLGA nanoparticles were suspended in a 500 µL of 3% PVA-PEMA (95:5) water phase. The nanoparticles suspension was then added into an oil phase containing 30 mg of PLGA (50:50) dissolved in 5 mL of Ethyl Acetate. The first emulsion was formed via homogenization at 9250 rpm for 20 seconds (FSH 125, Fisherbrand). The emulsion mixture was transferred into a 30 mL of 3% PVA-PEMA (95:5) water phase and homogenized at 6250 rpm for 2 minutes. The double emulsion mixture was then transferred into a 60 mL of 3% PVA-PEMA (95:5) water phase and stirred at 1200 rpm under a fume hood for 4 hours to ensure complete evaporation of the organic solvent. The formed MDS spheres were washed and collected via serial centrifugation (5810R, Eppendorf).

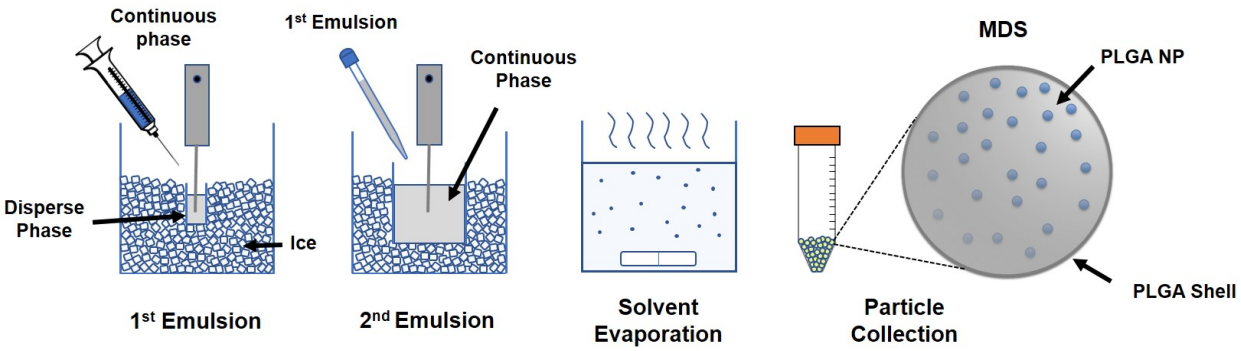

Figure 4.2: Synthesis of MDS by a double emulsification solvent evaporation method.

Nanoparticles loading into MDS carriers was confirmed using fluorescence microscopy (Eclipse, TS2R, Nikon). A scanning electron microscope (SEM Neoscope JCM-5000, Nikon) was used to verify morphology and loading of MDS. Encapsulation efficiency of PLGA nanoparticles into MDS capsules was estimated from the remaining nanospheres suspended in supernatant after MDS collection compared to an initial loading number of nanoparticles.

4.2.4 Isolation of RBCs, Cell-Free Plasma and Monocytes From Human Whole Blood

Human blood was collected via venipuncture according to a protocol approved by the Texas A&M University Internal Review Board and in line with the standards set by the Helsinki Declaration. Venous blood was obtained from healthy adult donors into a 30 ml syringe containing acetate-citrate-dextrose, ACD, as anticoagulant. RBCs were obtained by centrifugation of whole blood at 500 g for 10 minutes. The supernatant was removed and centrifuged at 2500 g for 10 minutes to remove platelets and leukocytes, and obtain cell-free plasma. Collected RBCs were washed with DPBS and centrifuged at 500 g for 10 mins prior to resuspending in DPBS at desired concentration.

Human peripheral blood monocytes were isolated from fresh human whole blood following a protocol provided by Alere Technologies AS, based on a Polymorphrep density gradient. Collected monocytes were pooled and cultured in tissue culture flasks pretreated with gelatin (0.2% w/v).

4.2.5 Culture of Human Umbilical Vein Endothelial Cells

Human umbilical vein endothelial cells (HUVECs) were purchased from Lonza. HUVECs were pooled and cultured following Lonzas recommended protocols. Briefly, HUVEC were cultured under sterile conditions until reaching confluence in a T75 flask pretreated with gelatin (0.2% w/v). Endothelial Growth Medium-2 (EGM-2 Medium) was also purchased from Lonza, containing EBM-2 Basal Medium supplemented with human Epidermal Growth Factor (hEGF), Vascular Endothelial Growth Factor (VEGF), R3-Insulin-like Growth Factor-1 (R3-IGF-1), Ascorbic Acid, Hydrocortisone, human Fibroblast Growth Factor-Beta (hFGF-β), Heparin, Fetal Bovine Serum (FBS), and Gentamicin/Amphotericin-B (GA).

4.2.6 MDS and Nanoparticle Cytotoxicity Study

HUVEC cells and peripheral blood monocytes were harvested via trypsinization and reseeded at a 5x10^5 cell density in a 96-wells microplate. After an overnight incubation, cells were treated with MDS loaded with chitosan coated nanoparticles at different concentrations and incubated for 4, 12, 24 and 72 hours. Untreated HUVEC and monocyte cells incubated under the same conditions were used as control. After each desired incubation time point, 10 µL of colorimetric cell counting kit-8 (CCK-8) reagent was added to each well and incubated for 4 hours at 37°C. The cells were then measured for an absorption at 450 nm using a plate reader. The cell viability was determined by comparing the recorded absorption intensity to a CCK-8 calibration curve, generated according to the manufacture recommendations.

4.2.7 Preparation of Ligand-Conjugated MDS and PLGA Nanoparticles

MDS capsules and nanoparticles were functionalized with targeting ligands via EDAC-carbodiimide chemistry and avidin-biotin linkages as described in chapter 3. Briefly, carboxylated MDS surface was initially modified with NeutrAvidin proteins in EDAC and MES buffer. Subsequently, biotinylated human sLea (or VCAM-1 antibody, aVCAM-1) was added to the NeutrAvidin conjugated MDS. The functionalized capsules were washed in DPBS, collected by centrifugation, and stored at 4°C in the dark until use. After conjugation, the PLGA-based MDS and nanoparticles were in-

cubated in DPBS+ and 1% BSA for 2 hours to block non-specific binding of spheres to secondary antibodies and endothelial cells.

For MDS capsules, the site density of sLea or aVCAM-1 on the MDS surface was determined by flow cytometry (FACSCalibur, Becton, Dickinson and Company). SLeA- and aVCAM-1- MDS were stained with human PE-labeled CLA secondary antibodies (antiCLA-PE) and FITC-labeled rabbit anti-Mouse IgG (H+L) secondary antibodies, respectively. Unstained MDS, avidin-coated MDS stained with the antiCLA-PE and the secondary antibodies, and isotype controls were used as controls. A number of ligand density was calculated using MESF PE and FITC calibration beads.

For nanoparticles, the ligand site density was evaluated by an ELISA assay. Avidin conjugated PLGA nanoparticles were incubated with biotin-labeled horseradish peroxidase (B-HRP) for 30 min. Particles were then washed with PBS to remove unbounded BHRP and then transferred into an opaque 96-well plate. Amplex Red fluorescent peroxidase was added to samples, allowing for a 10-min reaction. The fluorescent intensity of untreated (control) and amplex Red treated nanoparticles were measured using a microplate reader at 544 nm excitation/590 nm emission. MDS with a desired ligand site density was evaluated with the ELISA assay and used as a reference for estimating the ligand site density of nanoparticles relative to MDS.

4.2.8 In-Vitro Flow Adhesion Experiment

A straight channel formed inside of a rectangular parallel plate flow chamber (PPFC) was used for all in-vitro targeted-particle attachment assays. A silicon gasket with a rectangular opening was attached to the flow chamber deck. The rectangular opening in the silicon gasket determined the width and length dimensions of the flow channel while the gasket thickness defined the channel height. Experimental setup used to test the particle binding from a laminar flow was similar to previously described in [32] with minor modifications.

An endothelial cell monolayer was prepared by seeding HUVECs onto 30 mm glass cover slips precoated with 1% gelatin cross-linked with glutaraldehyde, and incubated at 37°C in a 5% CO_2 incubator until confluence, as previously described [32]. The HUVEC monolayer was then activated with IL-1β (10 ng/mL) for 4 hours and attached to the bottom of a circular parallel plate

flow chamber (GlycoTech) to form the bottom wall of the flow channel (Figure 4.3A).

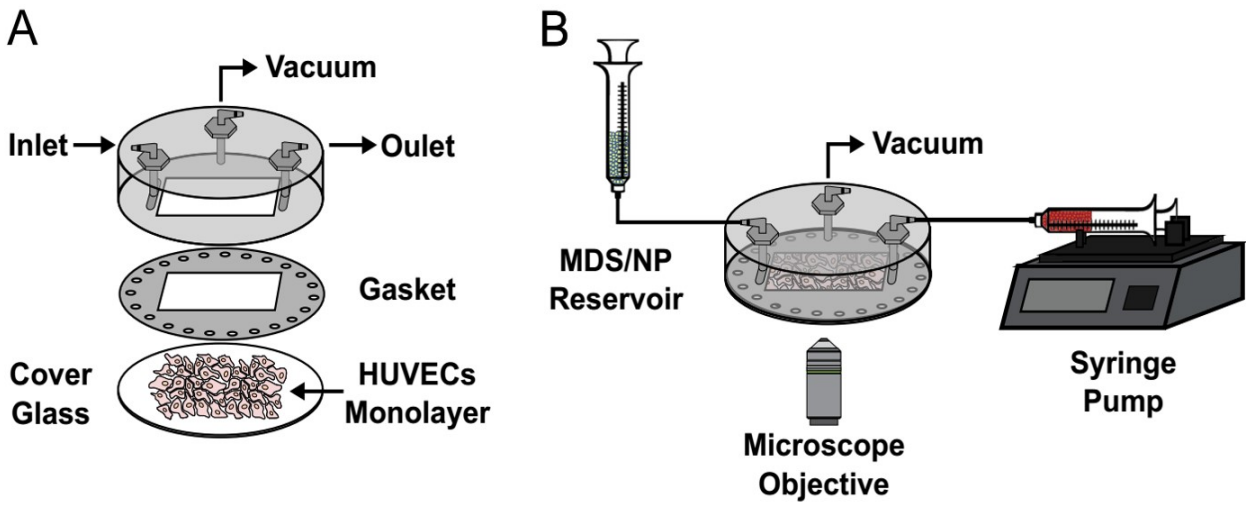

Figure 4.3: (A) Circular parallel plate flow chamber. (B) Experimental setup used to test particle binding under laminar flow conditions.

Next, sLeA-coated MDS were suspended in PBS saline or reconstituted blood (40% v/v of human red blood cells suspended in PBS) at 1x10^6 particles/mL, and introduced into the chamber with a laminar flow regulated through a programmable syringe pump (LEGATO 110, KD Scientific) (Figure 4.3B). Similarly, the binding efficiency under laminar flow conditions of MDS (3.6 μm) coated with sLeA was compared to functionalized PLGA nanoparticles (154 nm). MDS and nanoparticles were suspended in reconstituted blood (40% v/v of human red blood cells suspended in DPBS+) at 1x10^6 MDS/mL and 1.26x10^{10} nanoparticles/mL, respectively. The number of MDS and nanoparticles were adjusted to match the same drug-carrying volume.

The wall shear rate ($\gamma_w^{(s^{-1})}$)) in the flow channel was controlled to be 100 s^{-1} by adjusting the volumetric flow rate (Q) in accordance to:

$$\gamma_w^{(s^{-1})} = \frac{6Q}{h^2 w} \tag{4.1}$$

where Q is the volumetric flow rate (mL/min), h is the channel height (254 μm) and w is the channel width (1 cm).

Flow experiments were observed and recorded via a digital camera connected to an inverted light microscope (Eclipse, TS2R, Nikon). The microscope was located inside a temperature-controlled incubator in which a temperature was maintained at 37°C for all experiments. Adhesion of functionalized MDS to activated HUVEC cells was evaluated after 5 minutes of flow. The number of MDS carriers bound to endothelial cells was quantified and divided by the area covered by the cameras field of view. Data is presented as an average over at least 3 experiments and includes at least 5 fields of view per experiment.

4.3 Results

4.3.1 Chitosan-Coated PLGA Nanospheres

PLGA nanoparticles were fabricated using an oil-in-water (O/W) emulsion-solvent evaporation method. The varied level of mechanical energy produced by a homogenizer or a sonicator during the emulsification process generates various sizes of nanoparticles in a controllable manner. Table 4.1 shows the average diameter of prepared nanoparticles measured by nanoparticle-tracking analysis (NTA) technique. Nanoparticles can encapsulate both water soluble (i.e. methelyne blue) and water-insoluble (e.g. DiO) payloads. Figure 4.4 demonstrates morphology of nanoparticles via scanning-electron microscope (SEM).

Polymer	Payload	Avg. Diameter (nm)	Polymer	Payload	Avg. Diameter (nm)
PLGA (75:25)	**MB**	84 ± 30	PLGA (75:25)	**DiO**	78 ± 17
PLGA (75:25)	**MB**	128 ± 39	PLGA (75:25)	**DiO**	124 ± 22
PLGA (50:50)	**MB**	202 ± 22	PLGA (75:25)	**DiO**	206 ± 58
PLGA (50:50)	**MB**	338 ± 147	PLGA (75:25)	**DiO**	313 ± 110

Table 4.1: Average size of PLGA nanoparticles carrying methylene blue (MB) or DiO payloads.

To protect the integrity of the nanoparticles during subsequent encapsulation process within MDS, nanoparticles were coated with chitosan, a hydrophilic and positively charged polymer. Figure 4.5 shows the particle surface zeta potential change produced by chitosan coating. Chitosan

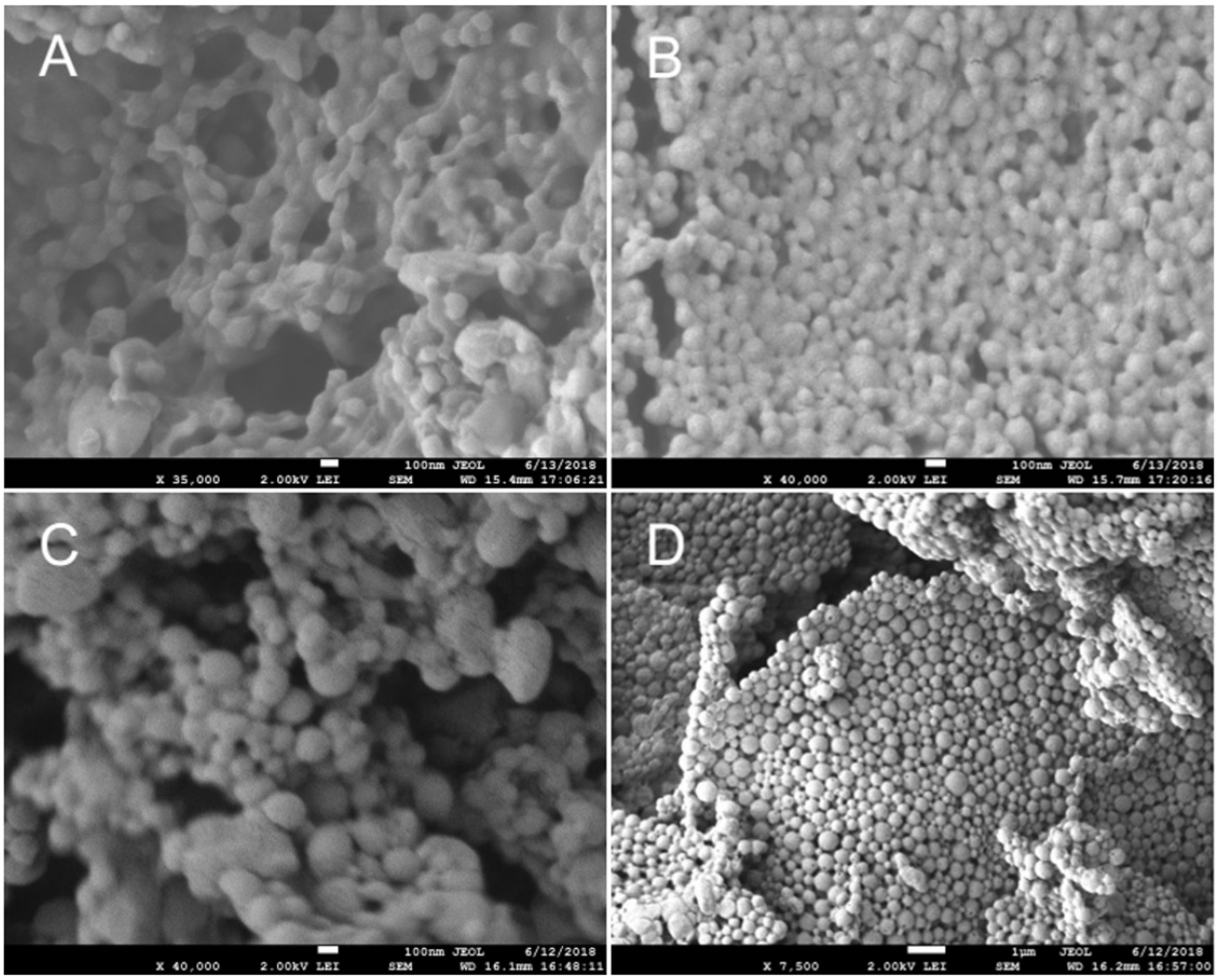

Figure 4.4: SEM images of PLGA nanoparticles loaded with payload surrogate (DiO fluorescent dye) with an average diameter of (A) 78 nm, (B) 125 nm, (C) 207 nm and (D) 313 nm.

also showed to help delaying and preventing premature payload release from nanoparticles particularly during the first 8 hours (Figure 4.5).

4.3.2 PLGA-Based Multistage Delivery Systems

PLGA-based MDS were fabricated using a double emulsion (water-inoil-in-water, W/O/W)-solvent evaporation technique. As described by [46], double emulsion solvent evaporation method allows the fabrication of particles with either capsule or honeycomb structures. If the difference of size between the first and the second emulsion droplets is big and the concentration of polymer is high, particles with inner honeycomb structures get formed (Figure 4.6D). In contrast, if the

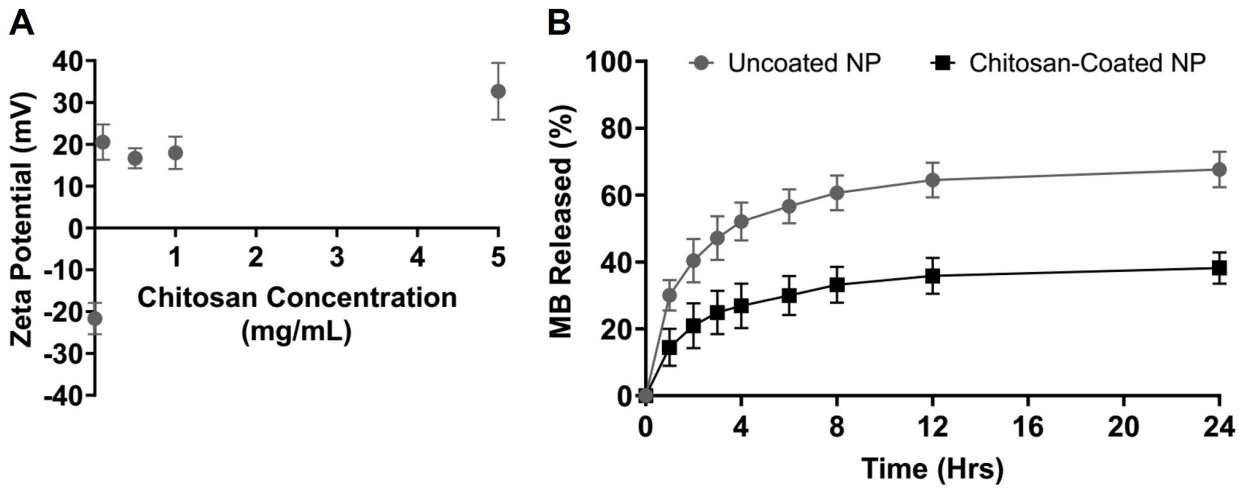

Figure 4.5: (A) Chitosan coating effect on PLGA nanoparticle surface zeta potential. (B) Methylene blue release profile of uncoated- and chitosan-coated nanoparticles in a saline buffer at 37°C.

diameters of the inner and outer droplets are very similar, then microcapsules are formed (Figure 4.6A-C).

The MDS were formed with an inner microcapsule structure, i.e. an outer microsphere shell that carries multiple nanoparticles. By optimizing fabrication conditions such as emulsion stirring speed, polymer concentration, and the ratio of oil/water in both emulsification steps, DiO-loaded nanoparticles with average diameters of 78, 125, 206 and 313 nm were successfully encapsulated into 4-7 μm MDS.As it can be observed on Figure 4.7, there was not significant difference in the size of MDS containing all three different sizes of nanoparticles, and the PLGA nanospheres remained inside of the MDS-shell. A rough estimation of DiO nanoparticles loaded into MDS capsules, suggest a correlation between the diameter of the encapsulated nanospheres and their entrapment efficiency into MDS. Depending on the applications, smaller nanoparticles may be desired for targeting deeper tissues while larger nanoparticles may be desired when a higher capacity of payloads is needed. Table 4.2 summarizes the average diameter of MDS loaded with chitosan coated PLGA nanoparticles.

The release profiles of nanoparticles from MDS was studied in a saline buffer (DPBS+) and human plasma under rotation and sink condition at 37°C. Figure 4.8 demonstrates the sustained

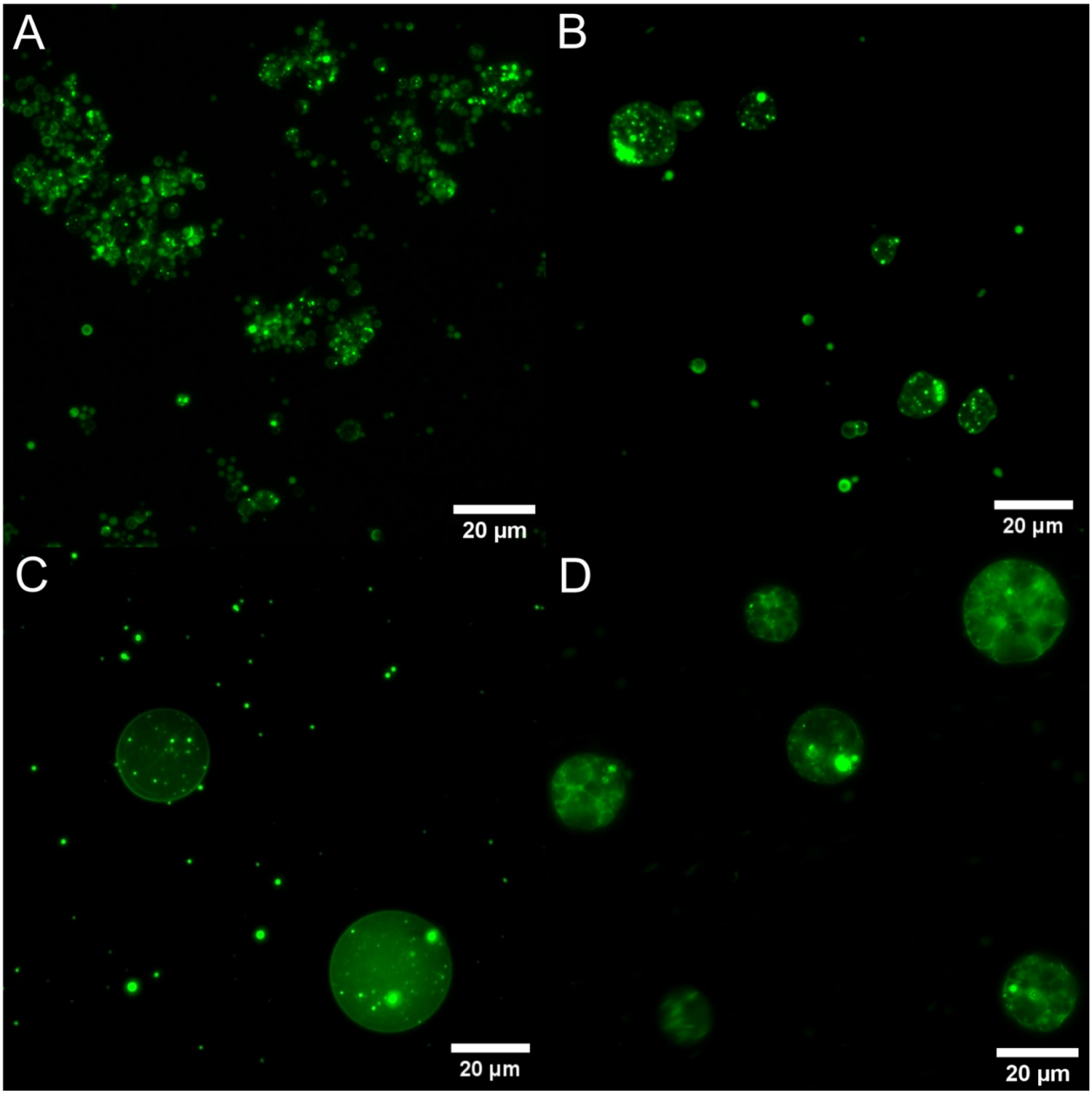

Figure 4.6: MDS loaded with DiO nanoparticles fabricated by a double emulsion solvent evaporation method. MDS synthesized using different second emulsion homogenization speeds: (A) 12,500 rpm, (B) 8,500 rpm and (C) 6,500 rpm. The difference of shear stress applied during second emulsion resulted on drastic differences on MDS final diameter. MDS shown on (D) were prepared using same parameters than (C) except by a much higher shear stress applied during the first emulsification resulting in a honeycomb structure.

release of the chitosan coated PLGA nanoparticles from MSD for more than 72 hours. A faster release rate was observed for MDS suspended in human plasma likely due to enzymatic activity

Nanoparticle Diameter	MDS Diameter	Loading (np/MDS)	Total NP
125 nm	**5.54 μm**	17	2.18×10^{10}
220 nm	**6.76 μm**	13	3.68×10^{9}
310 nm	**7.04 μm**	12	1.51×10^{9}

Table 4.2: Fabricated MDS carrying chitosan coated PLGA nanoparticles.

during incubation. These results suggest that the MDS microshell provides a protective isolation for nanoparticles allowing then to keep their integrity until are released from MDS.

PLGA-based nanospheres and MDS were tested for their biocompatibility with HUVECs and human primary monocytes using a cell-counting kit 8 (CCK-8) assay. Both MDS and PLGA nanoparticles showed to be safe to human endothelial cells and monocytes. Figure 4.9 shows that both nanospheres and MDS at 0.1 mg/mL and 1 mg/mL do not caused significant toxicity to human monocytes for up to 24 hours.

Similarly, Figure 4.10 demonstrates that MDS at 0.01 mg/mL, 0.1 mg/mL and 1 mg/mL do not cause significant toxicity to HUVEC cells up to 72 hours.

Sialyl-Lewis A were successfully immobilized to the MDS surface and enabled specific targeting to inflamed human endothelium. A flow cytometer shift of the particles stained with PE-secondary antibody confirmed SLeA conjugated to the MDS surface with a site density of 1374.25 sites/μm^2 (Figure 4.11A). Conjugation of PLGA-nanoparticles to SLeA ligands was verified by an ELISA essay. The fluorescence intensity measured from the secondary antibody suggest a 4-fold increase of the site density for nanoparticles compared to MDS (Figure 4.11B).

4.3.3 In-Vitro Flow Adhesion Experiment

MDS spheres with 3.6 μm average diameter were used to confirm the specificity of sLeA-functionalized MDS to activated human endothelial cells. Overall, these spheres coated with sLeA were easily captured to the surface of IL-1β-activated endothelial cells from flow in the presence or absence of RBCs in a parallel plate chamber as shown in Figure 4.12. As previously reported by [55], the presence of RBCs enhanced the adhesion of MDS to the activated endothelial cells surface

over MDS in buffer with no RBCs (DPBS+) (p=0.047). Control experiments with avidin-coated MDS showed no significant binding, thus confirming the specificity of the interaction between MDS and IL-1β-activated endothelial cells.

Similarly, PLGA nanoparticles coated with SLeA were introduced into the parallel plate chamber with a laminar flow profile. Their interaction with the activated HUVECs monolayer was recorded and compared with MDS results. SLeA-functionalized MDS consistently showed significantly better localization and attachment to the surface of the activated endothelial cells compared to the PLGA nanoparticles also coated with SLeA (p=0.0003) (Figure 4.12B). Previous studies demonstrated that particles with average diameters around 2 μm are optimal for vascular wall localization from laminar flow [32]. Control experiments with avidin-coated PLGA nanoparticles showed no significant attachment to the IL-1β-activated HUVECs monolayer.

4.3.4 Discussion

PLGA nanoparticles with diameters from 78 nm to 330 nm were successfully loaded into MDS. Our results suggest a correlation between the nanoparticles diameter and the total number of nanospheres loaded into MDS. No significant difference was found on average size of formed MDS when loaded with nanoparticles with different diameters (75 to 330 nm). Since MDS were fabricated with a microcapsule inner structure, degradation rates are expected to be much faster than solid-core and honeycomb PLGA microspheres [46]. This property could increase the capabilities of MDS as nanoparticle carrier, and enable the efficient and fast release of nanospheres at the targeted site.

As it was shown in chapter 2, PLGA nanoparticles present a much faster release rate compared to PLGA microspheres. Although, coating nanoparticles with a layer of chitosan, not just only provided them with a protective layer from the organic solvent during MDS fabrication, but also helped to delay their degradation rate. This extra layer of chitosan allowed nanoparticles to remain stable until they were released from MDS. Also, as previously reported [71, 72], particle surface zeta potential might enhance the cellular uptake of drug nanocarriers making them more suitable as therapeutic platforms.

Both MDS and chitosan coated nanospheres had no significant cytotoxicity to human monocytes for 24 hours and HUVECs for up to 72 hours. It is expected that PLGA-based MDS and nanoparticles would be suitable systems for the intravascular delivery of contrast agents, drugs or proteins since both PLGA and chitosan are biodegradable and biocompatible.

Laminar flow experiments, demonstrated the efficient attachment of sLeA-functionalized MDS that were easily captured to the surface of IL-1β-activated endothelial cells. Results shown on Figure 4.12A confirmed that the presence of RBCs enhanced the adhesion of MDS to the activated endothelial cells surface over particles in buffer with no RBCs (DPBS+), as previously reported [55]. Control experiments with avidin-coated MDS showed no significant binding, thus confirming the specificity of the interaction between MDS and IL-1β-activated endothelial cells.

As results on Figure 4.12B indicate, MDS coated with SLeA showed a superior attachment to the activated HUVECs monolayer compared to functionalized PLGA nanoparticles. These findings suggest a great potential for MDS as a drug delivery carrier, by enhancing the delivery of nanoparticles to the vascular wall. This multistage approach could reduce the accumulation of nanospheres in filtering organs and non-targeted tissues, and at the same time take advantage of the inherent properties of nanoparticles such as the ability to penetrate into deeper tissues, especially on health conditions such as cancer and atherosclerosis.

Overall, this research work shows that the development of this microcarrier delivery system can enhance the endothelial adhesion/internalization probability of nanospheres. Specifically, MDS provide promising capabilities as IV-administered microcarriers for MB-loaded nanospheres, to enable the delivery and targeting of atherosclerotic biomarkers in deeper arterial layers.

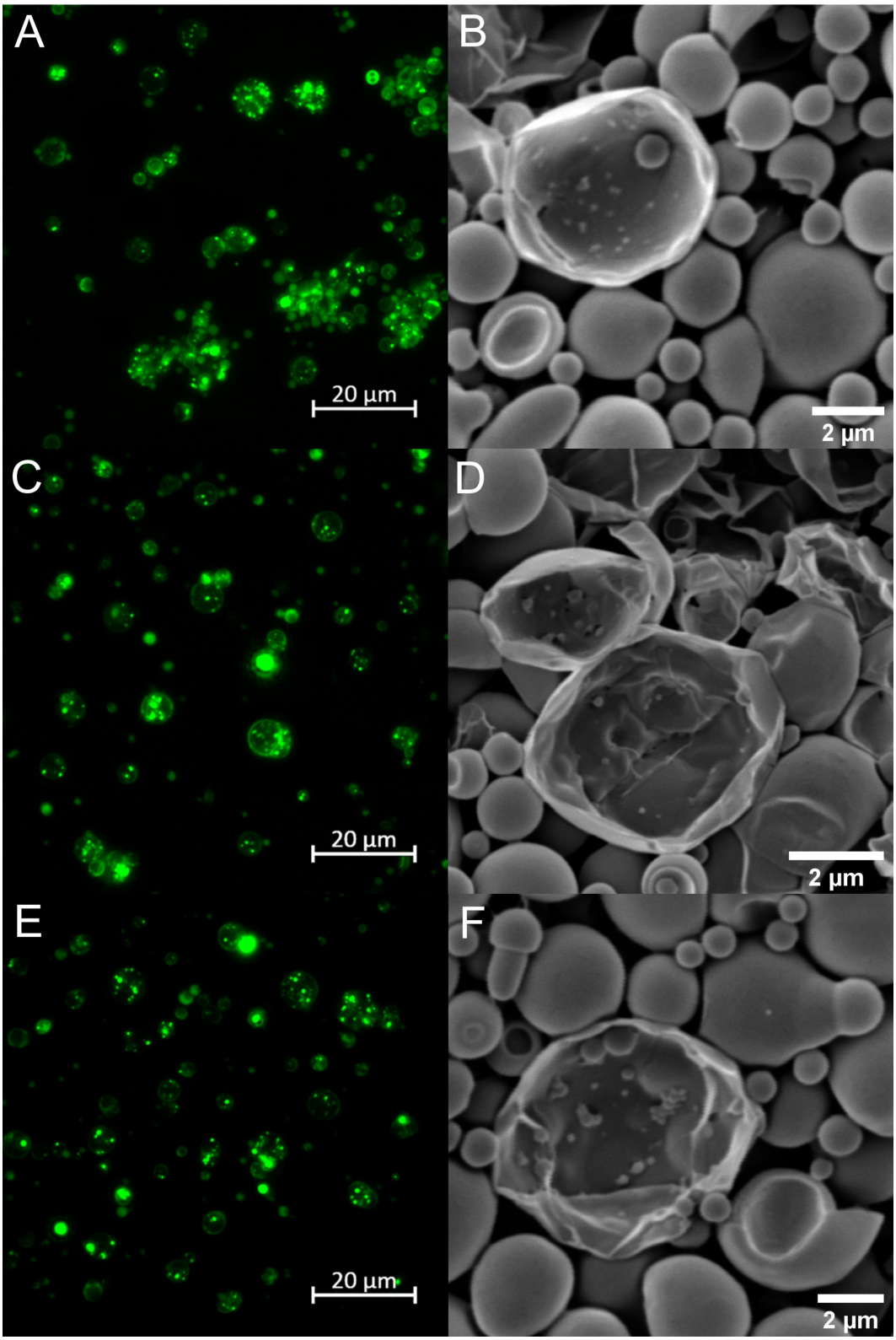

Figure 4.7: Fluorescent microscope images of MDS loaded with (A) 125 nm, (B) 206 nm and (C) 313 nm- DiO loaded nanoparticles. SEM cross-section images of MDS loaded with (D) 125 nm and (E) 313 nm DiO-loaded nanoparticles.

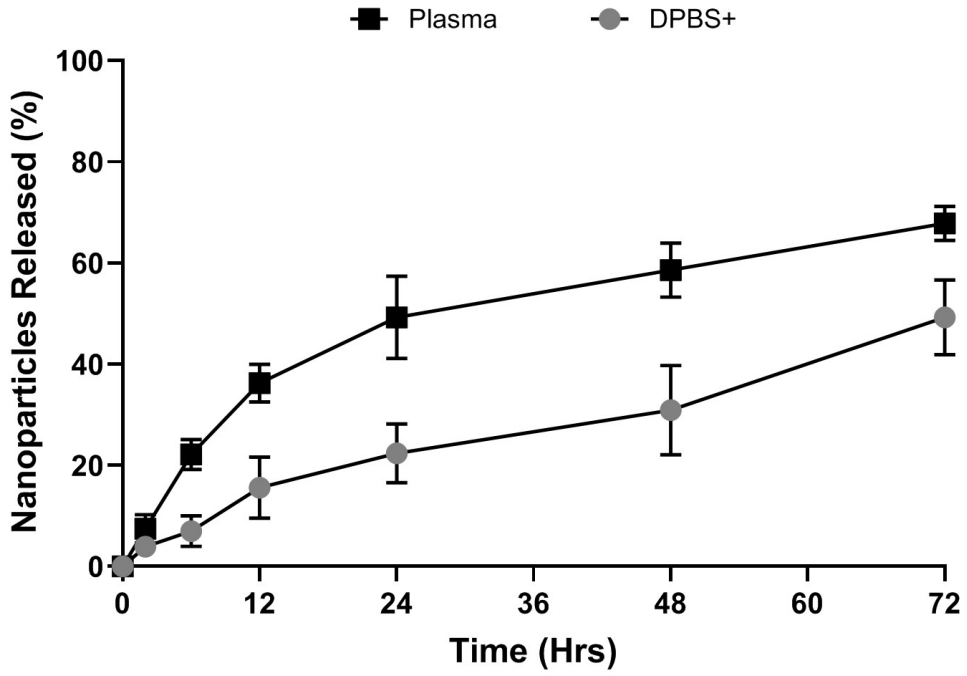

Figure 4.8: MDS release profile in DPBS+ and Human Plasma at 37°C.

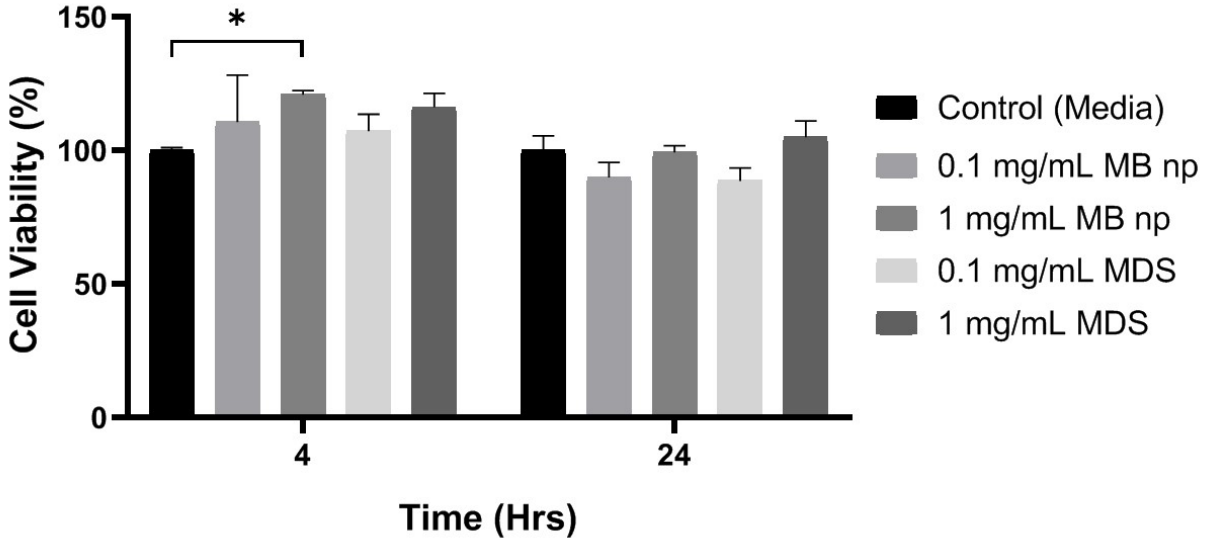

Figure 4.9: Human monocytes cytotoxicity studies. Black bars represent human monocyte cell viability treated with media (control). Value = mean $\pm$ SD (n = 3).

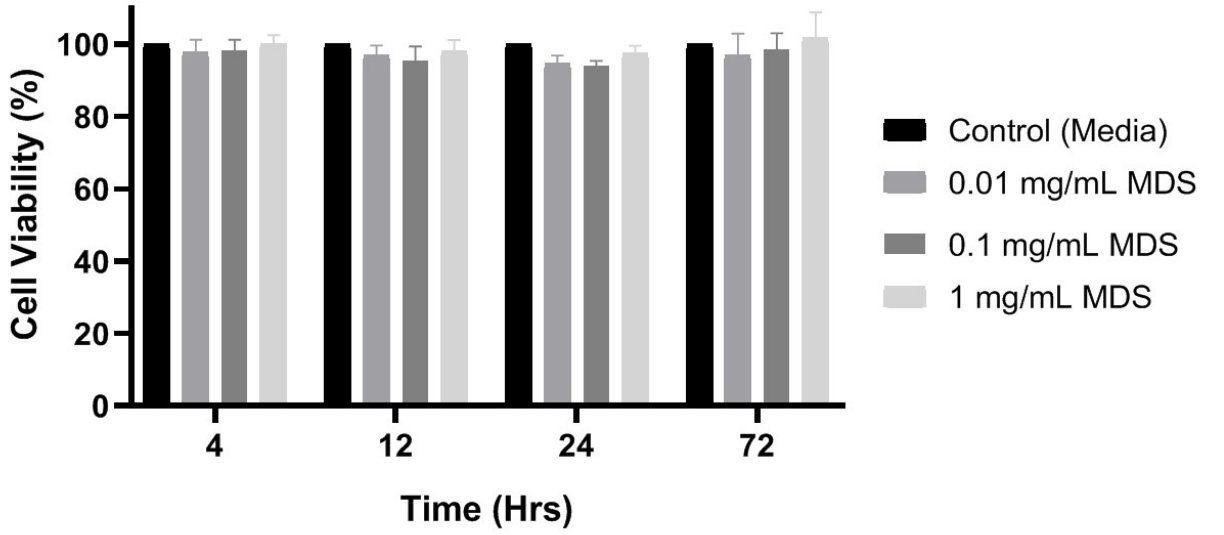

Figure 4.10: HUVECs viability treated with control (media) and MDS at different concentrations. Value = mean ± SD (n = 3).

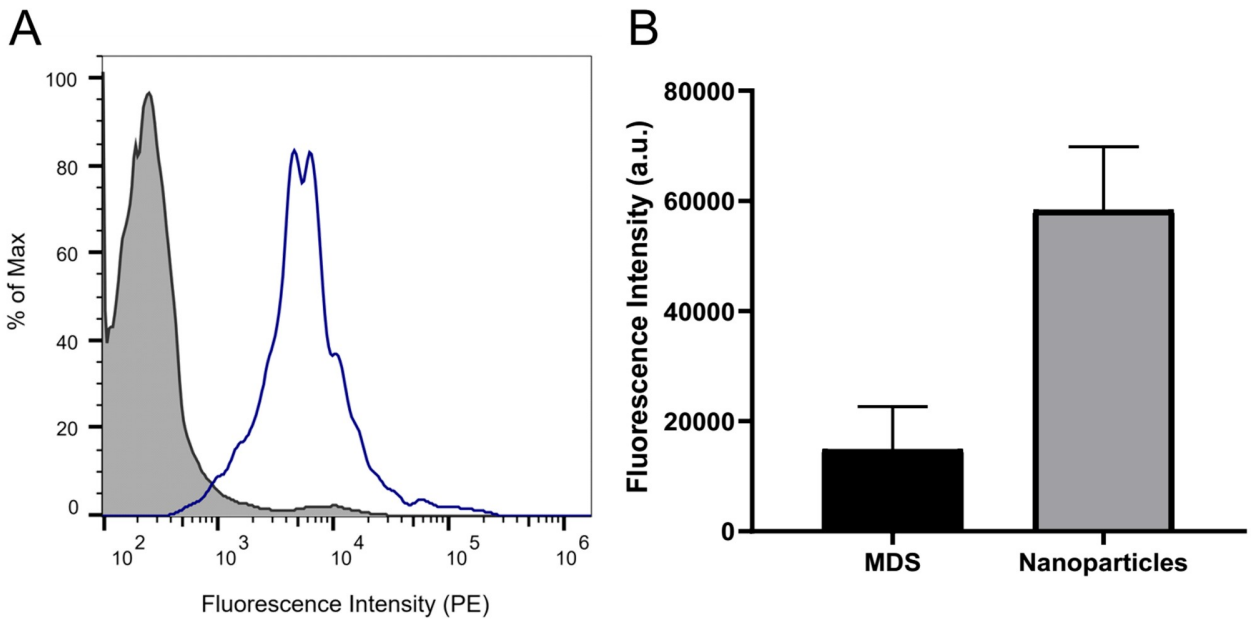

Figure 4.11: (A) Flow cytometry histogram of SLeA functionalized MDS labeled with a PE-secondary antibody (blue) and uncoated MDS (gray). (B) Fluorescence intensity from an ELISA essay of functionalized MDS and PLGA nanoparticles.

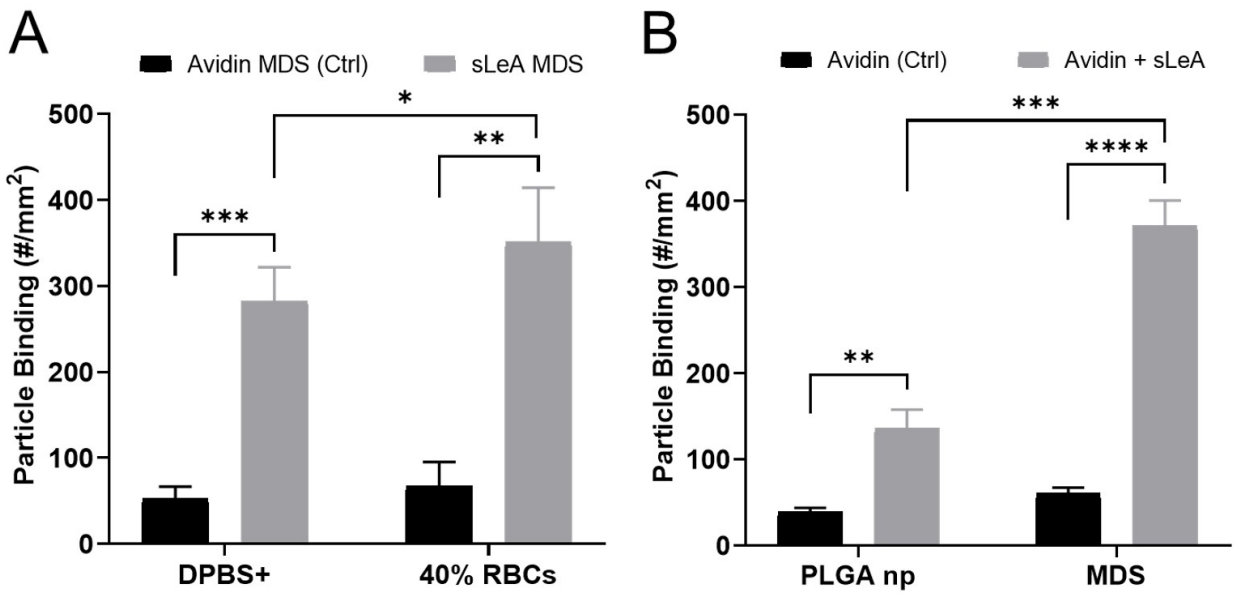

Figure 4.12: (A) Adhesion of sLeA or avidin-coated MDS to IL-1β-activated HUVECs monolayer under laminar flow in a parallel plate flow chamber and in the presence or absence of red blood cells (40% RBCs) (WSR = 100 s^{-1}). (B) Binding of MDS or PLGA nanoparticles, suspended in reconstituted blood (40% RBC), from flow to an activated HUVECs monolayer. Value = mean $\pm$ SD (n = 3).

5. CONCLUSIONS AND FUTURE WORK

5.1 Conclusions

In conclusion, we have developed a versatile molecular contrast agent for PPOCT by combining the advantages of a biodegradable polymer and the spectral properties of methylene blue that could provide specific labeling of biomarkers in multiple diseases. PLGA particles loaded with MB were successfully fabricated with broad average diameters range from 2.7 μm down to 84 nm. Fabrication parameters were optimized to reach encapsulation efficiencies above 48%. The enhancement of chemical and photo-stability of encapsulated MB was experimentally confirmed. To the best of our knowledge, this is the first time that MB loaded PLGA particles are used as PPOCT contrast agents. These results suggest that MB-PLGA spheres have the potential for labeling pathological biomarkers by using PPOCT imaging and hopefully enabling more accurate diagnostics.

PPOCT imaging of post-mortem human artery sections, allowed the identification of MB molecules encapsulated into PLGA micro and nanospheres targeted to VCAM-1, a biomarker for early stages of atherosclerotic plaques. MB molecules were driven into the triplet state using a pump light source centered at 660 nm. The modulated transient absorption of MB at 830 nm was recorded from frequency domain OCT M-scans. The average light power used while imaging was 3.8 mW, well under the ANSI maximum permissible exposure for skin. PPOCT imaging of MB-loaded particles offers a promising molecular imaging tool due to the great availability of ligands that can be attached to the PLGA particles surface to target very specific biomarkers.

Additionally, a new multistage delivery system was also developed to enhance the endothelial adhesion, delivery and internalization of contrast and drug-loaded nanocarriers. PLGA based MDSs were successfully formed with microcapsule inner structures and average diameters from 4 to 7 μm encapsulating chitosan coated PLGA nanoparticles. Results from in-vitro experiments such as MDS-nanoparticle release rate, cytotoxicity and endothelial specific binding, suggest a

great potential of these platforms as in-vivo targeted microcarriers for intravascular delivery of nano-size spheres.

5.2 Future Work

Though this dissertation has described the development molecular contrast agents for PPOCT and a MDS for endothelium targeted delivery of nanocarriers, which can have a significant impact on intravascular imaging, particularly for atherosclerotic plaque diagnosis, the investigation of these platforms could be further developed and extended in the following directions:

1) Further investigate the capabilities and limitations of these MB-PLGA micro and nanoparticles as high resolution molecular contrast agents for PPOCT imaging. Validate the specific labeling of atherosclerotic biomarkers by the developed MB-loaded PLGA particles on an in-vivo animal model.

2) Study the sustained delivery of nanoparticles from MDS into an endothelialized microfluidic device. A microfluidic device would need to be designed consisting of two-layers/chambers separated by a porous membrane on which endothelial cells would be grown. Internalization of delivered nanoparticles would be investigated.

REFERENCES

[1] T. Gambichler, G. Moussa, M. Sand, D. Sand, P. Altmeyer, and K. Hoffmann, "Applications of optical coherence tomography in dermatology," *J Dermatol Sci*, vol. 40, no. 2, pp. 85–94, 2005.

[2] F. Prati, E. Regar, G. S. Mintz, E. Arbustini, C. Di Mario, I. K. Jang, T. Akasaka, M. Costa, G. Guagliumi, E. Grube, Y. Ozaki, F. Pinto, P. W. Serruys, and O. C. T. R. D. Expert's, "Expert review document on methodology, terminology, and clinical applications of optical coherence tomography: physical principles, methodology of image acquisition, and clinical application for assessment of coronary arteries and atherosclerosis," *Eur Heart J*, vol. 31, no. 4, pp. 401–15, 2010.

[3] M. Adhi and J. S. Duker, "Optical coherence tomography–current and future applications," *Curr Opin Ophthalmol*, vol. 24, no. 3, pp. 213–21, 2013.

[4] G. Isenberg, J. Sivak, M. V., A. Chak, R. C. Wong, J. E. Willis, B. Wolf, D. Y. Rowland, A. Das, and A. Rollins, "Accuracy of endoscopic optical coherence tomography in the detection of dysplasia in barrett's esophagus: a prospective, double-blinded study," *Gastrointest Endosc*, vol. 62, no. 6, pp. 825–31, 2005.

[5] J. G. Fujimoto, C. Pitris, S. A. Boppart, and M. E. Brezinski, "Optical coherence tomography: An emerging technology for biomedical imaging and optical biopsy," *Neoplasia*, vol. 2, no. 1-2, pp. 9–25, 2000.

[6] J. Kim, W. Brown, J. R. Maher, H. Levinson, and A. Wax, "Functional optical coherence tomography: principles and progress," *Phys Med Biol*, vol. 60, no. 10, pp. R211–37, 2015.

[7] B. E. Applegate and J. A. Izatt, "Molecular imaging of endogenous and exogenous chromophores using ground state recovery pump-probe optical coherence tomography," *Opt Express*, vol. 14, no. 20, pp. 9142–55, 2006.

[8] K. D. Rao, M. A. Choma, S. Yazdanfar, A. M. Rollins, and J. A. Izatt, "Molecular contrast in optical coherence tomography by use of a pump-probe technique," *Optics Letters*, vol. 28, no. 5, pp. 340–342, 2003.

[9] O. Carrasco-Zevallos, R. L. Shelton, W. Kim, J. Pearson, and B. E. Applegate, "In vivo pump-probe optical coherence tomography imaging in xenopus laevis," *J Biophotonics*, vol. 8, no. 1-2, pp. 25–35, 2015.

[10] D. Jacob, R. L. Shelton, and B. E. Applegate, "Fourier domain pump-probe optical coherence tomography imaging of melanin," *Optics Express*, vol. 18, no. 12, pp. 12399–12410, 2010.

[11] W. Kim and B. E. Applegate, "In vivo molecular contrast oct imaging of methylene blue," *Opt Lett*, vol. 40, no. 7, pp. 1426–9, 2015.

[12] K. Orth, G. Beck, F. Genze, and A. Ruck, "Methylene blue mediated photodynamic therapy in experimental colorectal tumors in mice," *J Photochem Photobiol B*, vol. 57, no. 2-3, pp. 186–92, 2000.

[13] R. H. Schirmer, B. Coulibaly, A. Stich, M. Scheiwein, H. Merkle, J. Eubel, K. Becker, H. Becher, O. Muller, T. Zich, W. Schiek, and B. Kouyate, "Methylene blue as an antimalarial agent," *Redox Report*, vol. 8, no. 5, pp. 272–275, 2003.

[14] J. P. Tardivo, A. Del Giglio, C. S. de Oliveira, D. S. Gabrielli, H. C. Junqueira, D. B. Tada, D. Severino, R. de Fatima Turchiello, and M. S. Baptista, "Methylene blue in photodynamic therapy: From basic mechanisms to clinical applications," *Photodiagnosis Photodyn Ther*, vol. 2, no. 3, pp. 175–91, 2005.

[15] J. C. Lo, M. A. Darracq, and R. F. Clark, "A review of methylene blue treatment for cardiovascular collapse," *J Emerg Med*, vol. 46, no. 5, pp. 670–9, 2014.

[16] A. Matsui, E. Tanaka, H. S. Choi, V. Kianzad, S. Gioux, S. J. Lomnes, and J. V. Frangioni, "Real-time, near-infrared, fluorescence-guided identification of the ureters using methylene blue," *Surgery*, vol. 148, no. 1, pp. 78–86, 2010.

[17] S. Gioux, H. S. Choi, and J. V. Frangioni, "Image-guided surgery using invisible near-infrared light: Fundamentals of clinical translation," *Molecular Imaging*, vol. 9, no. 5, pp. 237–255, 2010.

[18] K. H. Song, E. W. Stein, J. A. Margenthaler, and L. V. Wang, "Noninvasive photoacoustic identification of sentinel lymph nodes containing methylene blue in vivo in a rat model," *J Biomed Opt*, vol. 13, no. 5, p. 054033, 2008.

[19] M. Jeon, W. T. Song, E. Huynh, J. Kim, J. Kim, B. L. Helfield, B. Y. C. Leung, D. E. Goertz, G. Zheng, J. Oh, J. F. Lovell, and C. Kim, "Methylene blue microbubbles as a model dual-modality contrast agent for ultrasound and activatable photoacoustic imaging," *Journal of Biomedical Optics*, vol. 19, no. 1, 2014.

[20] A. R. DiSanto and J. G. Wagner, "Pharmacokinetics of highly ionized drugs. ii. methylene blue–absorption, metabolism, and excretion in man and dog after oral administration," *J Pharm Sci*, vol. 61, no. 7, pp. 1086–90, 1972.

[21] M. Oz, D. E. Lorke, M. Hasan, and G. A. Petroianu, "Cellular and molecular actions of methylene blue in the nervous system," *Med Res Rev*, vol. 31, no. 1, pp. 93–117, 2011.

[22] J. M. May, Z. C. Qu, and C. E. Cobb, "Reduction and uptake of methylene blue by human erythrocytes," *Am J Physiol Cell Physiol*, vol. 286, no. 6, pp. C1390–8, 2004.

[23] D. Bechet, P. Couleaud, C. Frochot, M. L. Viriot, F. Guillemin, and M. Barberi-Heyob, "Nanoparticles as vehicles for delivery of photodynamic therapy agents," *Trends in Biotechnology*, vol. 26, no. 11, pp. 612–621, 2008.

[24] H. J. Hah, G. Kim, Y. E. Lee, D. A. Orringer, O. Sagher, M. A. Philbert, and R. Kopelman, "Methylene blue-conjugated hydrogel nanoparticles and tumor-cell targeted photodynamic therapy," *Macromol Biosci*, vol. 11, no. 1, pp. 90–9, 2011.

[25] X. He, X. Wu, K. Wang, B. Shi, and L. Hai, "Methylene blue-encapsulated phosphonate-terminated silica nanoparticles for simultaneous in vivo imaging and photodynamic therapy," *Biomaterials*, vol. 30, no. 29, pp. 5601–9, 2009.

[26] M. Qin, H. J. Hah, G. Kim, G. Nie, Y. E. Lee, and R. Kopelman, "Methylene blue covalently loaded polyacrylamide nanoparticles for enhanced tumor-targeted photodynamic therapy," *Photochem Photobiol Sci*, vol. 10, no. 5, pp. 832–41, 2011.

[27] J. Yu, C. H. Hsu, C. C. Huang, and P. Y. Chang, "Development of therapeutic au-methylene blue nanoparticles for targeted photodynamic therapy of cervical cancer cells," *ACS Appl Mater Interfaces*, vol. 7, no. 1, pp. 432–41, 2015.

[28] J. M. Lu, X. Wang, C. Marin-Muller, H. Wang, P. H. Lin, Q. Yao, and C. Chen, "Current advances in research and clinical applications of plga-based nanotechnology," *Expert Rev Mol Diagn*, vol. 9, no. 4, pp. 325–41, 2009.

[29] S. Mao, Y. Shi, L. Li, J. Xu, A. Schaper, and T. Kissel, "Effects of process and formulation parameters on characteristics and internal morphology of poly(d,l-lactide-co-glycolide) microspheres formed by the solvent evaporation method," *Eur J Pharm Biopharm*, vol. 68, no. 2, pp. 214–23, 2008.

[30] E. Sah and H. Sah, "Recent trends in preparation of poly(lactide-co-glycolide) nanoparticles by mixing polymeric organic solution with antisolvent," *Journal of Nanomaterials*, 2015.

[31] X. R. Song, Y. Zhao, S. X. Hou, F. Y. Xu, R. Zhao, J. Y. He, Z. Cai, Y. B. Li, and Q. H. Chen, "Dual agents loaded plga nanoparticles: Systematic study of particle size and drug entrapment efficiency," *European Journal of Pharmaceutics and Biopharmaceutics*, vol. 69, no. 2, pp. 445–453, 2008.

[32] P. Charoenphol, S. Mocherla, D. Bouis, K. Namdee, D. J. Pinsky, and O. Eniola-Adefeso, "Targeting therapeutics to the vascular wall in atherosclerosis–carrier size matters," *Atherosclerosis*, vol. 217, no. 2, pp. 364–70, 2011.

[33] J. M. Tarbell, "Shear stress and the endothelial transport barrier," *Cardiovasc Res*, vol. 87, no. 2, pp. 320–30, 2010.

[34] Y. Kim, M. E. Lobatto, T. Kawahara, B. Lee Chung, A. J. Mieszawska, B. L. Sanchez-Gaytan, F. Fay, M. L. Senders, C. Calcagno, J. Becraft, M. Tun Saung, R. E. Gordon, E. S. Stroes,

M. Ma, O. C. Farokhzad, Z. A. Fayad, W. J. Mulder, and R. Langer, "Probing nanoparticle translocation across the permeable endothelium in experimental atherosclerosis," *Proc Natl Acad Sci U S A*, vol. 111, no. 3, pp. 1078–83, 2014.

[35] N. C. Chesler and O. C. Enyinna, "Particle deposition in arteries ex vivo: effects of pressure, flow, and waveform," *J Biomech Eng*, vol. 125, no. 3, pp. 389–94, 2003.

[36] M. J. Heslinga, E. M. Mastria, and O. Eniola-Adefeso, "Fabrication of biodegradable spheroidal microparticles for drug delivery applications," *J Control Release*, vol. 138, no. 3, pp. 235–42, 2009.

[37] C. Cannava, R. Stancanelli, M. R. Marabeti, V. Venuti, C. Cascio, P. Guarneri, C. Bongiorno, G. Sortino, D. Majolino, A. Mazzaglia, S. Tommasini, and C. A. Ventura, "Nanospheres based on plga/amphiphilic cyclodextrin assemblies as potential enhancers of methylene blue neuroprotective effect," *Rsc Advances*, vol. 6, no. 20, pp. 16720–16729, 2016.

[38] V. Klepac-Ceraj, N. Patel, X. Song, C. Holewa, C. Patel, R. Kent, M. M. Amiji, and N. S. Soukos, "Photodynamic effects of methylene blue-loaded polymeric nanoparticles on dental plaque bacteria," *Lasers Surg Med*, vol. 43, no. 7, pp. 600–6, 2011.

[39] M. E. Keegan, J. L. Falcone, T. C. Leung, and W. M. Saltzman, "Biodegradable microspheres with enhanced capacity for covalently bound surface ligands," *Macromolecules*, vol. 37, no. 26, pp. 9779–9784, 2004.

[40] W. Tang, H. Xu, E. J. Park, M. A. Philbert, and R. Kopelman, "Encapsulation of methylene blue in polyacrylamide nanoparticle platforms protects its photodynamic effectiveness," *Biochemical and Biophysical Research Communications*, vol. 369, no. 2, pp. 579–583, 2008.

[41] H. Sakai, B. Li, W. L. Lim, and Y. Iga, "Red blood cells donate electrons to methylene blue mediated chemical reduction of methemoglobin compartmentalized in liposomes in blood," *Bioconjug Chem*, vol. 25, no. 7, pp. 1301–10, 2014.

[42] G. Schafer and H. S. Penefsky, "Bioenergetics: energy conservation and conversion . introduction," *Results Probl Cell Differ*, vol. 45, pp. IV–VIII, 2008.

[43] D. Gabrielli, E. Belisle, D. Severino, A. J. Kowaltowski, and M. S. Baptista, "Binding, aggregation and photochemical properties of methylene blue in mitochondrial suspensions," *Photochem Photobiol*, vol. 79, no. 3, pp. 227–32, 2004.

[44] D. Severino, H. C. Junqueira, M. Gugliotti, D. S. Gabrielli, and M. S. Baptista, "Influence of negatively charged interfaces on the ground and excited state properties of methylene blue," *Photochem Photobiol*, vol. 77, no. 5, pp. 459–68, 2003.

[45] E. Morgounova, Q. Shao, B. J. Hackel, D. D. Thomas, and S. Ashkenazi, "Photoacoustic lifetime contrast between methylene blue monomers and self-quenched dimers as a model for dual-labeled activatable probes," *Journal of Biomedical Optics*, vol. 18, no. 5, 2013.

[46] I. D. Rosca, F. Watari, and M. Uo, "Microparticle formation and its mechanism in single and double emulsion solvent evaporation," *J Control Release*, vol. 99, no. 2, pp. 271–80, 2004.

[47] N. Sharma, P. Madan, and S. S. Lin, "Effect of process and formulation variables on the preparation of parenteral paclitaxel-loaded biodegradable polymeric nanoparticles: A co-surfactant study," *Asian Journal of Pharmaceutical Sciences*, vol. 11, no. 3, pp. 404–416, 2016.

[48] A. Budhian, S. J. Siegel, and K. I. Winey, "Haloperidol-loaded plga nanoparticles: systematic study of particle size and drug content," *Int J Pharm*, vol. 336, no. 2, pp. 367–75, 2007.

[49] X. Song, Y. Zhao, W. Wu, Y. Bi, Z. Cai, Q. Chen, Y. Li, and S. Hou, "Plga nanoparticles simultaneously loaded with vincristine sulfate and verapamil hydrochloride: systematic study of particle size and drug entrapment efficiency," *Int J Pharm*, vol. 350, no. 1-2, pp. 320–9, 2008.

[50] G. S. Singhal and Rabinowi.E, "Changes in absorption spectrum of methylene blue with ph," *Journal of Physical Chemistry*, vol. 71, no. 10, p. 3347, 1967.

[51] H. K. Makadia and S. J. Siegel, "Poly lactic-co-glycolic acid (plga) as biodegradable controlled drug delivery carrier," *Polymers (Basel)*, vol. 3, no. 3, pp. 1377–1397, 2011.

[52] R. W. Redmond and J. N. Gamlin, "A compilation of singlet oxygen yields from biologically relevant molecules," *Photochem Photobiol*, vol. 70, no. 4, pp. 391–475, 1999.

[53] M. C. DeRosa and R. J. Crutchley, "Photosensitized singlet oxygen and its applications," *Coordination Chemistry Reviews*, vol. 233, pp. 351–371, 2002.

[54] W. Tang, H. Xu, R. Kopelman, and M. A. Philbert, "Photodynamic characterization and in vitro application of methylene blue-containing nanoparticle platforms," *Photochemistry and Photobiology*, vol. 81, no. 2, pp. 242–249, 2005.

[55] P. Charoenphol, R. B. Huang, and O. Eniola-Adefeso, "Potential role of size and hemodynamics in the efficacy of vascular-targeted spherical drug carriers," *Biomaterials*, vol. 31, no. 6, pp. 1392–402, 2010.

[56] Y. Yeo and K. N. Park, "Control of encapsulation efficiency and initial burst in polymeric microparticle systems," *Archives of Pharmacal Research*, vol. 27, no. 1, pp. 1–12, 2004.

[57] N. V. Jyothi, P. M. Prasanna, S. N. Sakarkar, K. S. Prabha, P. S. Ramaiah, and G. Y. Srawan, "Microencapsulation techniques, factors influencing encapsulation efficiency," *J Microencapsul*, vol. 27, no. 3, pp. 187–97, 2010.

[58] R. Alex and R. Bodmeier, "Encapsulation of water-soluble drugs by a modified solvent evaporation method. i. effect of process and formulation variables on drug entrapment," *J Microencapsul*, vol. 7, no. 3, pp. 347–55, 1990.

[59] R. Bonnett, "Photosensitizers of the porphyrin and phthalocyanine series for photodynamic therapy," *Chemical Society Reviews*, vol. 24, no. 1, pp. 19–33, 1995.

[60] E. J. Benjamin, P. Muntner, A. Alonso, M. S. Bittencourt, C. W. Callaway, A. P. Carson, A. M. Chamberlain, A. R. Chang, S. Cheng, S. R. Das, F. N. Delling, L. Djousse, M. S. V. Elkind, J. F. Ferguson, M. Fornage, L. C. Jordan, S. S. Khan, B. M. Kissela, K. L. Knutson, T. W. Kwan, D. T. Lackland, T. T. Lewis, J. H. Lichtman, C. T. Longenecker, M. S. Loop, P. L. Lutsey, S. S. Martin, K. Matsushita, A. E. Moran, M. E. Mussolino, M. O'Flaherty, A. Pandey, A. M. Perak, W. D. Rosamond, G. A. Roth, U. K. A. Sampson, G. M. Satou,

E. B. Schroeder, S. H. Shah, N. L. Spartano, A. Stokes, D. L. Tirschwell, C. W. Tsao, M. P. Turakhia, L. B. VanWagner, J. T. Wilkins, S. S. Wong, S. S. Virani, E. American Heart Association Council on, C. Prevention Statistics, and S. Stroke Statistics, "Heart disease and stroke statistics-2019 update: A report from the american heart association," *Circulation*, vol. 139, no. 10, pp. e56–e528, 2019.

[61] R. Ladeiras-Lopes, S. Agewall, A. Tawakol, B. Staels, E. Stein, R. J. Mentz, A. Leite-Moreira, F. Zannad, and W. Koenig, "Atherosclerosis: Recent trials, new targets and future directions," *Int J Cardiol*, vol. 192, pp. 72–81, 2015.

[62] J. M. Tarkin, M. R. Dweck, N. R. Evans, R. A. Takx, A. J. Brown, A. Tawakol, Z. A. Fayad, and J. H. Rudd, "Imaging atherosclerosis," *Circ Res*, vol. 118, no. 4, pp. 750–69, 2016.

[63] J. E. Phipps, D. Vela, T. Hoyt, D. L. Halaney, J. J. Mancuso, L. M. Buja, R. Asmis, T. E. Milner, and M. D. Feldman, "Macrophages and intravascular oct bright spots: a quantitative study," *JACC Cardiovasc Imaging*, vol. 8, no. 1, pp. 63–72, 2015.

[64] J. A. Jo, J. Park, P. Pande, S. Shrestha, M. J. Serafino, J. Rico Jimenez Jde, F. Clubb, B. Walton, L. M. Buja, J. E. Phipps, M. D. Feldman, J. Adame, and B. E. Applegate, "Simultaneous morphological and biochemical endogenous optical imaging of atherosclerosis," *Eur Heart J Cardiovasc Imaging*, vol. 16, no. 8, pp. 910–8, 2015.

[65] M. G. Sorci-Thomas and M. J. Thomas, "Microdomains, inflammation, and atherosclerosis," *Circ Res*, vol. 118, no. 4, pp. 679–91, 2016.

[66] A. Phinikaridou, M. E. Andia, A. Protti, A. Indermuehle, A. Shah, A. Smith, A. Warley, and R. M. Botnar, "Noninvasive magnetic resonance imaging evaluation of endothelial permeability in murine atherosclerosis using an albumin-binding contrast agent," *Circulation*, vol. 126, no. 6, pp. 707–19, 2012.

[67] L. Tang, N. P. Gabrielson, F. M. Uckun, T. M. Fan, and J. Cheng, "Size-dependent tumor penetration and in vivo efficacy of monodisperse drug-silica nanoconjugates," *Mol Pharm*, vol. 10, no. 3, pp. 883–92, 2013.

[68] L. J. Cruz, M. A. Stammes, I. Que, E. R. van Beek, V. T. Knol-Blankevoort, T. J. A. Snoeks, A. Chan, E. L. Kaijzel, and C. Lowik, "Effect of plga np size on efficiency to target traumatic brain injury," *J Control Release*, vol. 223, pp. 31–41, 2016.

[69] R. E. Serda, J. Gu, R. C. Bhavane, X. Liu, C. Chiappini, P. Decuzzi, and M. Ferrari, "The association of silicon microparticles with endothelial cells in drug delivery to the vasculature," *Biomaterials*, vol. 30, no. 13, pp. 2440–8, 2009.

[70] S. S. Feng, G. Ruan, and Q. T. Li, "Fabrication and characterizations of a novel drug delivery device liposomes-in-microsphere (lim)," *Biomaterials*, vol. 25, no. 21, pp. 5181–9, 2004.

[71] B. S. Kim, C. S. Kim, and K. M. Lee, "The intracellular uptake ability of chitosan-coated poly (d,l-lactide-co-glycolide) nanoparticles," *Arch Pharm Res*, vol. 31, no. 8, pp. 1050–4, 2008.

[72] K. Tahara, T. Sakai, H. Yamamoto, H. Takeuchi, N. Hirashima, and Y. Kawashima, "Improved cellular uptake of chitosan-modified plga nanospheres by a549 cells," *Int J Pharm*, vol. 382, no. 1-2, pp. 198–204, 2009.